

Article

Characteristics and Formation Mechanism of the Lower Paleozoic Dolomite Reservoirs in the Dongying Depression, Bohai Bay Basin

Xuemei Zhang ^{1,2}, Qing Li ^{1,2,*}, Xuelian You ³, Lichi Ma ⁴, Anyu Jing ⁴, Wen Tian ⁴ and Lang Wen ^{1,2}

¹ State Key Laboratory of Petroleum Resources and Prospecting, China University of Petroleum (Beijing), Beijing 102249, China; 2019210099@student.cup.edu.cn (X.Z.); 2019210100@student.cup.edu.cn (L.W.)

² College of Geosciences, China University of Petroleum (Beijing), Beijing 102249, China

³ School of Ocean Science, China University of Geosciences (Beijing), Beijing 100083, China; youxuelian@cugb.edu.cn

⁴ Exploration and Production Research Institute of Shengli Oilfield Company, Sinopec, Dongying 257001, China; malichi.slyt@sinopec.com (L.M.); jinganyu.slyt@sinopec.com (A.J.); tianwen755.slyt@sinopec.com (W.T.)

* Correspondence: liqing@cup.edu.cn

Abstract: The Lower Paleozoic carbonate strata experience multi-stage tectonic activity and post-depositional volcanic activity in the Dongying Depression, Bohai Bay basin. These tectonic and magmatic activities have caused the reservoir to undergo severe diagenesis, resulting in strong reservoir heterogeneity. This study aims to identify the characteristics of dolomite, various reservoir spaces' characteristics, the origin of different types of dolomite, and the porosity evolution. According to crystal size and morphology, dolomites can be divided into three kinds of matrix dolomites and four kinds of dolomite cements. The petrology and geochemistry of the dolomite suggests that matrix dolomite is formed from seawater. The medium-to-coarse-crystalline dolomite cement (D3) has a higher $^{87}\text{Sr}/^{86}\text{Sr}$ ratio (0.7119 to 0.7129) and a higher homogenization temperature ($>125\text{ }^{\circ}\text{C}$), suggesting that the fluid for the precipitation of D3 is a mixed fluid formed by hydrothermal fluid eroding the ^{87}Sr -rich feldspar sandstone. The strikingly negative $\delta^{18}\text{O}$ values (-23.7 to $-25.7\text{ }_{\text{‰}}$ VPDB) of saddle dolomite (D4) indicate that D4 precipitated from hydrothermal fluids and the Mg^{2+} source may be due to dissolution of the host dolomite that formed in the evaporation environment. The reservoir spaces of the target strata in the study area mainly include fractures, dissolution vugs, intercrystalline pores, and moldic pores. Dissolution is the basis for forming high-quality dolomite reservoirs. The faults and fractures provided favorable conditions for dissolution. Hydrothermal fluid and organic acid were the main dissolution fluids for the dolomite reservoir, which were beneficial to the development of secondary pores. In the study area, organic acid dissolution was shown to contribute more than hydrothermal dissolution in the study area.

Keywords: buried hill reservoir; the lower Paleozoic; dolomitization; diagenesis; pore evolution



Citation: Zhang, X.; Li, Q.; You, X.; Ma, L.; Jing, A.; Tian, W.; Wen, L. Characteristics and Formation Mechanism of the Lower Paleozoic Dolomite Reservoirs in the Dongying Depression, Bohai Bay Basin. *Energies* **2022**, *15*, 2155. <https://doi.org/10.3390/en15062155>

Academic Editors: Yuming Liu and Bo Zhang

Received: 11 January 2022

Accepted: 11 March 2022

Published: 16 March 2022

Publisher's Note: MDPI stays neutral with regard to jurisdictional claims in published maps and institutional affiliations.



Copyright: © 2022 by the authors. Licensee MDPI, Basel, Switzerland. This article is an open access article distributed under the terms and conditions of the Creative Commons Attribution (CC BY) license (<https://creativecommons.org/licenses/by/4.0/>).

1. Introduction

Dolomite reservoirs are important hydrocarbon reservoirs. According to the statistics of 226 large–medium-scale carbonate hydrocarbon fields, dolomite reservoirs account for 90% of the world's carbonate hydrocarbon fields [1,2]. The development of the dolomite reservoirs is also related to the changes in climate that took place during the geological period. Older carbonate strata commonly have higher ratios of dolomite reservoirs [3]. Domestically, dolomite reservoirs are located in the Majiagou Formation in the northern Ordos Basin [4], in the Qixia and Dengying Formation and in the Sichuan Basin [5–9], in the Changxing–Feixian Formation in the Puguang Oilfield, and in the Lower Paleozoic in the Tarim Basin [10].

As for the genesis of dolomite reservoirs, most dolomite reservoirs are considered to have been initially formed by reflux dolomitization in an arid climate environment and

capillary concentration [11,12]. Furthermore, assuming that there was enough Mg^{2+} and a dynamic mechanism, this microbial-induced dolomitization can also occur in carbonate formations [13,14]. Since the 1990s, hydrothermal dolomitization and buried dolomitization under the deep-buried environments have been proposed by scholars [15–19]. Additionally, dolomitization under high-temperature and deep-buried environments might improve the permeability and porosity of dolomite reservoirs [20].

Previous studies have suggested that carbonate rocks are more susceptible to the alteration of multi-type and multi-stage diagenesis during diagenetic evolution. The development of reservoir spaces and the quality of the late physical properties are significantly controlled by diagenesis [21,22]. Carbonate reservoirs that have been influenced by the diagenesis have more complicated pore evolution [23–25]. In recent years, the qualities of carbonate rock reservoirs have been the focus of many studies [26]. There are several types of diagenesis that affect the reservoir properties of carbonate rocks, including dolomitization, fracturing, dissolution, compaction, and cementation. Dolomitization, dissolution, and fracturing are the main constructive types of reservoir diagenesis [22,27,28], while cementation and compaction represent the destructive forms of reservoir diagenesis [29,30]. In recent years, research on carbonate diagenesis has mainly focused on the structurally controlled hydrothermal alteration of carbonate reservoirs, and studies have pointed out that the effects of tectonic-controlled hydrothermal alteration on reservoirs are multifaceted [15,31–33]. Therefore, it is difficult to clearly delineate the time boundaries of different types of diagenesis. Meanwhile, studies still present some doubts regarding the dissolution mechanism of carbonate minerals by deep hydrothermal fluids [34].

In the last few decades, many studies have been carried out on the carbonate reservoir in the Paleozoic strata of the Dongying Depression [35], many of which have focused on the reservoir characteristics of the buried hill zone in the western portion of the depression and the Caoqiao-Guangrao buried hill zone in particular [36], and these studies have proposed that carbonate reservoirs can be divided into the two following categories: weathering crust-type buried hills and inner dissolution-type buried hills [37]. The development of these carbonate reservoirs was mainly controlled by karstification and fracture development, and it has been suggested that the dolomite formations are more likely to form high-quality reservoirs [38]. Dolomite reservoirs have been explored in the Ordovician Badou Formation in the Zhuanghai area, which were previously predicted to be favorable reservoir areas [39]. In recent years, the dolomite reservoir of the Yeli-Liangjiashan Formation has also become a key exploration target in the Shengli Oilfield, especially in the Zhuanghai area [40]. Most studies have concluded that dissolution and dolomitization are the key factors for forming favorable reservoirs. However, there are insufficient studies on the lower Paleozoic carbonate reservoirs in the Gaoqing-pingnan area. There is little research on dolomite reservoirs and dolomite cement types in this area.

Although scholars have studied the southwest area of the Dongying Depression, most of these studies have focused on the influence of atmospheric fresh water on buried hill reservoirs. However, these ignored the fact that the matrix dolomite and dolostone cement are the most important factors influencing the formation of high-quality reservoirs. Therefore, this study focuses on the matrix dolomite and all types of dolostone cement of the Lower Paleozoic formation in the southwest of the Dongying Depression. The major goals of this study are to (1) analyze the genesis of the dolostone cements, diagenesis, and the pore evolution characteristics under the different diagenesis, utilizing petrographic, geochemical data; (2) carry out the study on the relationship between diagenesis and reservoir pore evolution in the study area. This study is conducive to understanding the reservoir characteristics and their distribution laws, providing some geological basis for later exploration.

2. Geological Setting

The Dongying Depression is located on the southeast of the Jiyang Sag, with an area of 5700 km² [41] and mostly faces northeast. The Dongying Depression belongs to a sub-

tectonic unit in the Jiyang Sag, Bohai Bay Basin [42]. The study area mainly comprises the Gaoqing-Pingnan area in the southwest of the Dongying Depression (Figure 1a). The southern upper plate of the Gaoqing fault belongs to the Gaoqing uplift, and the eastern falling plate belongs to the Boxing depression [43].

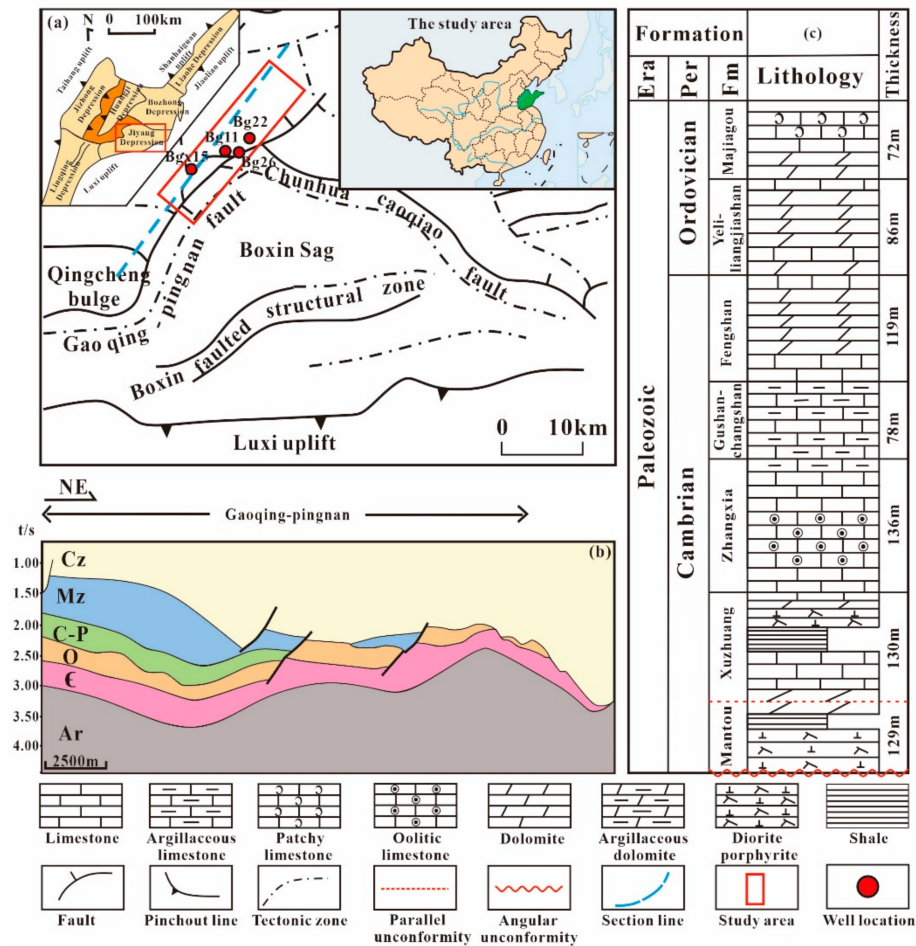


Figure 1. (a) Tectonic setting of the Dongying Depression, Bohai Bay Basin; (b) characteristics of formation development in NE-trending strata profile; section line is shown in (a); (c) stratigraphy of the Lower Paleozoic Formation in Dongying Depression, Bohai Bay Basin (modified after [44]). The map of China is quoted from [45].

In the study area, the Lower Paleozoic carbonate strata have experienced multiple periods of tectonic activity and post-depositional volcanic activity. Tectonic activity in the study area is divided into two main periods. The first large tectonic activity occurred during the Indosinian (Late Permian–Triassic period). The tectonic activity in the Indosinian period caused strong denudation of the Paleozoic strata in the relatively uplifted area of the study area. The second large-scale tectonic activity occurred in the Yanshan period (Jurassic–Early Cretaceous period). This tectonic activity was an extremely frequent and violent tectonic activity following the Indosinian period, and this tectonic activity was also accompanied by strong volcanic activity.

The objective strata consist of the Lower Paleozoic Ordovician and Cambrian carbonate reservoir [46]. The Cambrian strata consist of the Mantou Formation, Maozhuang Formation, Zhangxia Formation, Gushan Formation, Changshan Formation, and Fengshan Formation. The whole Cambrian is about 10–760 m thick. The Ordovician strata include the Yeli-Liangjiashan Formation, Majiagou Formation, and Badou Formation. The Ordovician strata is about 20–240 m thick [47]. The Badou Formation is missing from the study area due to uplift and denudation (Figure 1b,c). Due to the strata of uplift that took place during

the tectonic activity period, Carboniferous and Permian strata are absent in the higher parts of the structure. Therefore, the Lower Paleozoic strata is in contact with the overlying Mesozoic unconformity [48].

The sedimentary facies in the Paleozoic portions of the Dongying Depression comprise clastic sedimentary facies series and carbonate sedimentary facies series according to sedimentary rock types. The clastic sedimentary facies series were formed in supratidal and intertidal flat environments. The clastic sedimentary facies series can be further divided into mud flat and sand beach sedimentary subfacies according to their environment and lithology. Due to the decrease in the terrigenous material supply, the study area is mainly composed of argillaceous dolomite or limestone deposits. In one section of the study area, shale and mudstone are interbedded with dolomite and limestone. Carbonate sedimentary facies series can be further divided into evaporative platform facies, restricted platform facies, and open platform facies. The sedimentary facies comprise supratidal and intertidal zones from the Mantou and Xuzhuang periods, the main lithology is composed of oolitic limestone interbedded with shale; high-energy subtidal shoals and open seas were widely developed during the Zhangxia and Gushan periods. Intertidal flat and restricted sea facies were widely developed during the Changshan and the Early Ordovician periods. The main rock types comprise argillaceous limestone, silty limestone, and dolomite. The deposited environment gradually changed to shallow-water supratidal and intertidal zones and deeper-water subtidal zones during the Middle Ordovician period [44,48].

The Dongying Depression is a fault depression basin that was developed on the background of bedrock paleotopography. This basin went through stable lifting during the Paleozoic period, fold uplifting during the Triassic to middle Jurassic periods, preliminary fault depression between the late Jurassic and Cretaceous periods, and rifting and spreading in the Cenozoic periods, resulting in whole depression [44,49]. These complex tectonic activities laid the foundation for the formation of multiple diageneses. Additionally, the magmatic hydrothermal activity that accompanied these tectonic activities provided a source of materials for the development of hydrothermal cement.

3. Analytical Methods

All samples were collected from the southwest section of the Dongying Depression, specifically in the Gaoqing-pingnan area. Wells Bg 26, Bg 22, Bgx 15, and Bg 11 were included for sample collection (Figure 1a). A total of 70 thin sections were half-stained with a mixture of potassium ferricyanide and alizarin red to qualitatively discriminate between dolomite types, which was carried out according to the different petrographic characteristics of the different dolomites after they had been stained (Table 1).

Cathodoluminescence (CL) analysis was performed at the Analytical Laboratory of the Beijing Research Institute of Uranium Geology (BRIUG) to determine the cement generations.

The oxygen and carbon stable isotope analyses were carried out at the Analytical Laboratory of the Beijing Research Institute of Uranium Geology (BRIUG). Carbonate powders were reacted with 100% phosphoric acid for 4 h at 25 °C for calcite and at 50 °C for dolomite, and the resultant CO₂ was measured to determine its oxygen and carbon isotopic ratios on a Delta plus mass spectrometer. The isotope values were determined relative to the Vienna Pee Dee Belemnite standard (VPDB). Reported in the standard notation relative to standard VPDB for carbonate ratios and VSMOW for oxygen ratios. $\delta^{18}\text{O}$ (VSMOW) values were converted to $\delta^{18}\text{O}$ (VPDB) values. The reproducibility values of the isotopic measurements for both C and O were better than $\pm 0.06\%$ and $\pm 0.08\%$, respectively.

Table 1. Information on the samples used in this study.

Well	Sample Depth (m)	Formation	Lithology Description	Sample Analysis	
Bg26	2515.6	Yeli-Liangjiashan	Limestone	Microscopic observation	
Bg26	2790.5	Zhangxia	Oolitic limestone	Microscopic observation	
Bg26	2791.2		Bioclastic limestone	C, O isotope; $^{87}\text{Sr}/^{86}\text{Sr}$	
Bg26	2791.5			Microscopic observation	
Bg26	2793.2			C, O isotope; $^{87}\text{Sr}/^{86}\text{Sr}$	
Bg26	2795.4			Microscopic observation	
Bg26	2795.5			Grain limestone	Cathodoluminescence
Bg26	2798.2			Dolomitic bioclastic limestone	C, O isotope; $^{87}\text{Sr}/^{86}\text{Sr}$
Bg26	2801.9			Calcareous dolomite	C, O isotope; $^{87}\text{Sr}/^{86}\text{Sr}$; Cathodoluminescence
Bg26	2803.5			Algal limestone	Microscopic observation
Bg22	2211.17		Ordovician	Microcrystalline dolomite	Microscopic observation
Bg22	2219.27	Microscopic observation			
Bg22	2233.04	C, O isotope; $^{87}\text{Sr}/^{86}\text{Sr}$			
Bg22	2236.4	C, O isotope; $^{87}\text{Sr}/^{86}\text{Sr}$			
Bg22	2236.76	Argillaceous dolomite		Microscopic observation	
Bg22	2246.89	Microcrystalline dolomite		Microscopic observation	
Bg22	2348.95	Microcrystalline dolomite		C, O isotope	
Bg22	2398	Fine-crystalline dolomite		Microscopic observation	
Bg22	2399.1			C, O isotope	
Bgx15	2238.9	Ordovician		Microcrystalline dolomite	C, O isotope
Bg11	2233.04	Ordovician	Microcrystalline dolomite	$^{87}\text{Sr}/^{86}\text{Sr}$; Cathodoluminescence	
Bg11	2434.5			C, O isotope	
Bg11	2435.24		Argillaceous limestone	C, O isotope; $^{87}\text{Sr}/^{86}\text{Sr}$	
Bg11	2449.5			Cathodoluminescence	

The $^{87}\text{Sr}/^{86}\text{Sr}$ isotope ratios were determined for selected matrix dolomite and dolomite cements using a Thermal Ionization Mass Spectrometer (TIMS, Phoenix) at the analytical Laboratory of the Beijing Research Institute of the Uranium Geology (BRIUG). The analytical precision of the individual runs was determined to be 0.00005 (2σ). The mean standard

error of the mass spectrometer performance was ± 0.00003 for standard GB/T 17672-1999. The measured $^{87}\text{Sr}/^{86}\text{Sr}$ isotope values were normalized using the following formula

$$(^{87}\text{Sr}/^{86}\text{Sr})_{\text{St}} = (^{87}\text{Sr}/^{86}\text{Sr})_{\text{Sa}} \times (1 + 2f) \quad (1)$$

$$f = [(^{87}\text{Sr}/^{86}\text{Sr})_{\text{St}} / (^{87}\text{Sr}/^{86}\text{Sr})_{\text{Sa}}] \div 2 \quad (2)$$

$$(^{87}\text{Sr}/^{86}\text{Sr})_{\text{Nor}} = (^{87}\text{Sr}/^{86}\text{Sr})_{\text{Sa}} \times (1 + f) \quad (3)$$

where $(^{87}\text{Sr}/^{86}\text{Sr})_{\text{St}}$ is the standard $^{87}\text{Sr}/^{86}\text{Sr}$ values, $(^{87}\text{Sr}/^{86}\text{Sr})_{\text{St}} = 8.37521$; $(^{87}\text{Sr}/^{86}\text{Sr})_{\text{Sa}}$ is the measured value of samples; $(^{87}\text{Sr}/^{86}\text{Sr})_{\text{Nor}}$ is the normalized value of samples.

In this work, the primary fluid inclusions of the dolomite and calcite in the fractures and vugs were selected for systematic microscopic temperature measurement. Fluid inclusion microthermometry measurements were carried out using a microscopic heating and cooling stage (Linkam THMSG600) at the Institute of Geology Chinese Academy of Geological Science, and the measurements were taken within a temperature range of -196 to $+600$ °C and at a test accuracy between ± 0.5 °C and ± 2 °C. The temperatures of the fluid inclusions were obtained by freezing and warming. First, liquid nitrogen was used to cool the fluid inclusions. The changes that took place in the fluid inclusions during the temperature drop were observed. The inclusions were slowly warmed back up after freezing. When performing the homogenization temperature measurements, the heating rate was 5 °C/min, and the changes in the two gas–liquid phases were observed during the heating process. The heating rate was controlled to 1 °C/min in order to accurately record the homogenization temperature when the first phase was close to disappearing.

4. Results

4.1. Petrography

Based on the core, thin section observation, the dolomites were able to be divided into two types: matrix dolomite and dolomite cements. The matrix dolomite mainly included argillaceous dolomite (M1), microcrystalline dolomite (M2), and fine-crystalline dolomite (M3). The dolomite cement filling the fractures and vugs included powder-to-fine-crystalline dolomite cement (D1), fine-crystalline ferroan dolomite cement (D2), medium-to-coarse-crystalline dolomite cement (D3), and saddle dolomite (D4).

4.1.1. Argillaceous Dolomite (M1)

In this type of dolomite, the crystals were smaller in size, less than 10 μm , with a euhedral–subhedral texture. There was no development of intercrystalline pores or intercrystalline dissolution pores between the dolomite crystals. The fractures were filled with seepage silt or clay minerals during uplift periods (Figure 2a,b). Argillaceous dolomite is commonly found in Middle Ordovician strata.

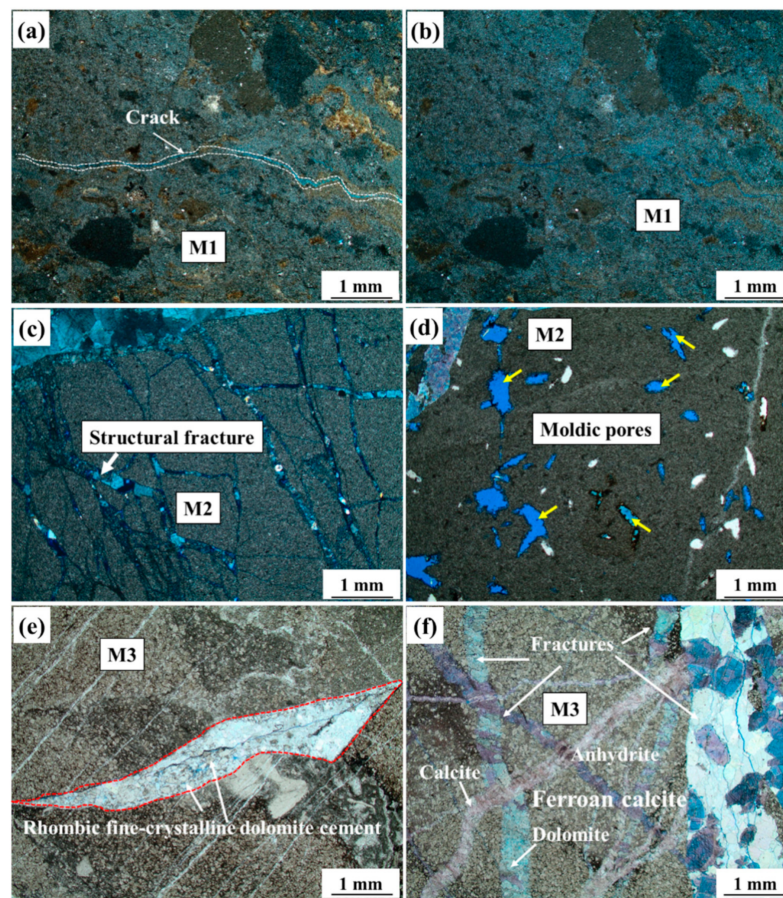


Figure 2. Petrological characteristics of various matrix dolomites in the Lower Paleozoic strata in the Dongying Depression, Bohai Bay Basin. (a) Argillaceous dolomite (M1), Well Bg22 2236.67 m, Ordovician formation, plane-polarized light; (b) same field of view as A, orthogonal light; (c) microcrystalline dolomite (M2), Well Bg22 2211.17 m, Ordovician formation, the structural fractures developed and filled by dolomite, orthogonal light; (d) microcrystalline dolomite (M2), Well Bg22 2233.04 m, Ordovician formation, dissolution vugs are developed, plane-polarized light; (e) fine-crystalline dolomite (M3), Well Bg22 2398 m, Ordovician formation, plane-polarized light; (f) multi-stage fractures are developed in fine-crystalline dolomite, Well Bg22 2399.1 m, Ordovician formation, plane-polarized light.

4.1.2. Microcrystalline Dolomite (M2)

This type of dolomite is defined as having a dolomite mineral of more than 90% in the dolomite rocks. This type of dolomite also shows the development of fractures, which are filled by medium-coarse-crystalline dolomite cements (Figure 2c). As the burial depth increases, selective dissolution vugs can be observed in the microcrystalline dolomite (Figure 2d). Microcrystalline dolomite mainly developed in the middle to lower parts of the Ordovician strata.

4.1.3. Fine-Crystalline Dolomite (M3)

This type of dolomite is defined as having a dolomite mineral content of more than 90% in the dolomite rocks, and the dolomite mainly comprises euhedral–subhedral crystals. Fine-crystalline dolomite is larger than 100 μm . Anhydrite cements can be seen, and part of the rhombic fine-crystalline dolomite is dispersed in the anhydrite cements (Figure 2e), indicating that the dolomite may have been formed by evaporation in an arid environment. Structural fractures developed in the fine-crystalline dolomite, which were successively filled with dolomite, calcite, and anhydrite (Figure 2f).

4.1.4. Powder-to-Fine-Crystalline Dolomite Cements (D1)

This type of dolomite cement is different from the fine-crystalline matrix dolomite. According to the different occurrence characteristics of the powder-to-fine-crystalline dolomite cements (D1), it can be divided into three types: (1) Most of the powder-to-fine-crystalline dolomites are distributed along stylolite (Figure 3a–c). Powder-to-fine-crystalline dolomite is about 46 μm in size. Powder-to-fine-crystalline dolomite cements (D1) are commonly rhomboid crystals and tend to have a euhedral structure, allowing them to form more intercrystalline pores. This type of dolomite is commonly nonluminous under the CL (Figure 4b). (2) The other type of powder-to-fine-crystalline dolomite mainly comprises the dolomite patches found in limestone and has euhedral crystals and poorer sorting (Figure 3e). This dolomite ranges from 39 μm to 88 μm in size. (3) Powder-to-fine-crystalline dolomite cements fill in the oolites. The early fluid selectively dissolved the interior of the oolite, and the late Mg-rich fluid recrystallized into the interior of the oolite to form rhombic dolomite crystals (Figure 3f). This dolomite ranges from 69 to 218 μm in size. Its crystals are usually characterized by “mist core bright edges” and are commonly nonluminous under the CL, only faint dull red cathodoluminescence can be seen at the edges of these dolomite crystals (Figure 4d). This type of dolomite is mainly distributed in the Zhangxia Formation of the Cambrian strata.

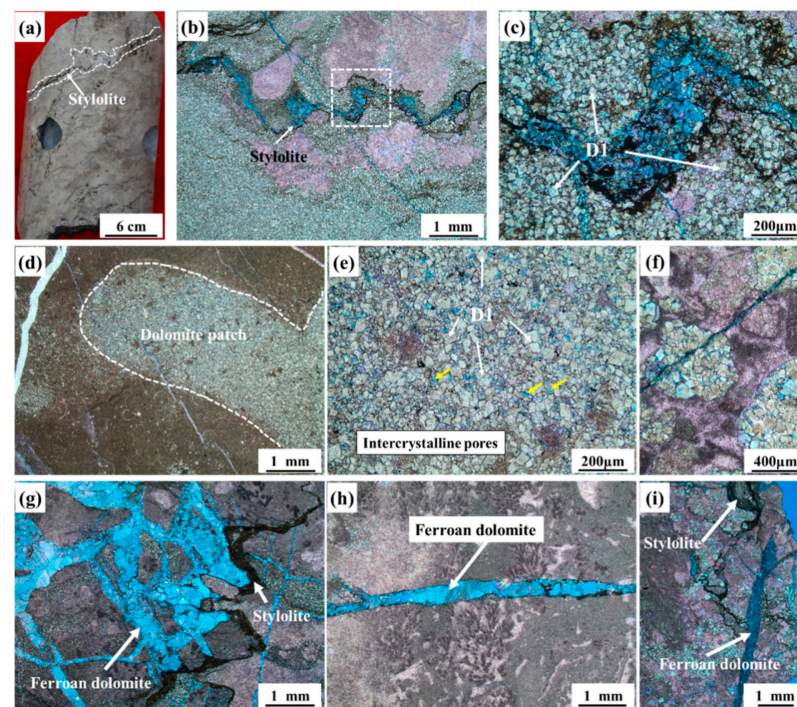


Figure 3. Petrological characteristics of the powder-fine dolomite and dolomite cements (D1). (a) Lower angle stylolite in the core, Well Bg26 2801.9 m, Zhangxia formation; (b) the characteristics of the powder-to-fine-crystalline dolomite cements (D1) around the stylolite. Stylolite is filled with black organic matter, Well Bg26 2801.9 m, Zhangxia formation; (c) local amplification of b; (d) the characteristics of the dolomite patch, the outside of the dolomite patch is argillaceous limestone, Well Bg26 2515.6 m, Yeli-Liangjiashan formation; (e) local amplification of d, intercrystalline pores (yellow arrow); (f) the characteristics of the powder-to-fine-crystalline dolomite cements (D1) interior of the oolite, Well Bg26 2790.5 m, Zhangxia formation; (g) the petrological characteristics of the fine-crystalline ferroan dolomite cement (D2) and the relationship between the fracture and stylolite, Well Bg26 2801.9 m, Zhangxia formation; (h) algal limestone. The petrological characteristics of the fine-crystalline ferroan dolomite cement (D2), Well Bg26 2803.5 m, Zhangxia formation; (i) dolomitic bioclastic limestone. The petrological characteristics of the fine-crystalline ferroan dolomite cement (D2), Well Bg26 2803.7 m, Zhangxia formation.

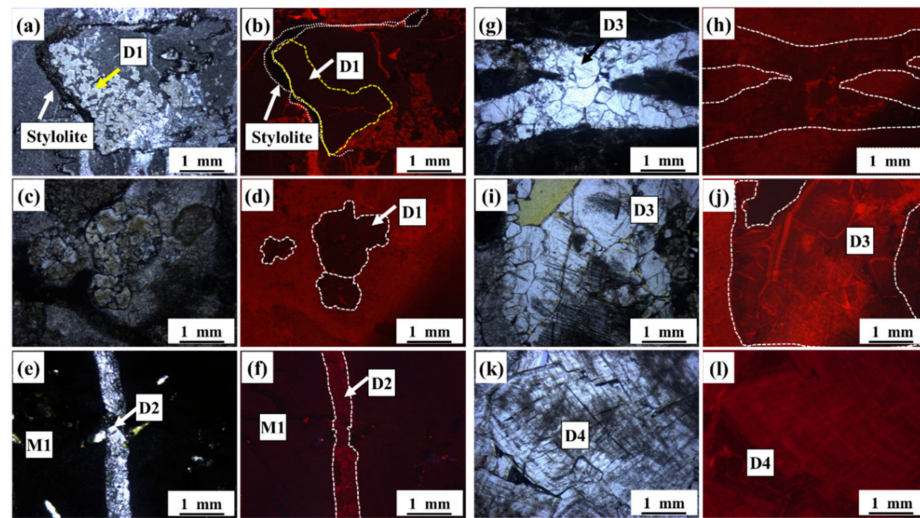


Figure 4. Thin section and the cathodoluminescence photomicrographs showing different kinds of dolomite cements in the Lower Paleozoic strata in the Dongying Depression, Bohai Bay Basin. (a) The powder-to-fine-crystalline dolomite cements (D1) along with the stylolite, Well Bg11 2449.5 m, Ordovician formation, plane-polarized light; (b) characteristics of cathodoluminescence in the same field of view as a. The powder-to-fine-crystalline dolomite cements within the yellow dotted line, CL; (c) the powder-to-fine-crystalline dolomite cements (D1) filled in the oolite and have the characteristics of “mist core bright edges”, Well Bg26 2795.5 m, Zhangxia formation, plane-polarized light; (d) the powder-fine-crystalline dolomite cements (D1) filled in the oolite within the white dotted line. The powder-fine-crystalline dolomite cements (D1) filled in the oolite in the same field of view as c, within the white dotted line, CL; (e) fractures developed in the microcrystalline dolomite (M2), which were filled in with fine-crystalline ferroan dolomite cements (D2), Well Bg22 2233.04, Ordovician formation, plane-polarized light; (f) characteristics of cathodoluminescence in the same field of view as e, and there are fine-crystalline ferroan dolomite cements (D2) in the white dotted line showing the weak dark red cathodoluminescence characteristics, CL; (g) the medium-to-coarse-crystalline dolomite cements (D3) filled in the fractures, Well Bg26 2801.9 m, Zhangxia formation, plane-polarized light; (h) characteristic of cathodoluminescence of the medium-to-coarse-crystalline dolomite cement (D3) filled in the fractures in the same field of view as g, and showing the weak cathodoluminescence, CL; (i) the characteristics of the medium-to-coarse-crystalline dolomites (D3) filled in the fractures, Well Bg26 2795.5 m, Zhangxia formation, plane-polarized light; (j) characteristics of cathodoluminescence of the medium-to-coarse-crystalline dolomite cements (D3) in the same field of view as i. The medium-to-coarse-crystalline dolomite cements with the obvious luminous bands, CL; (k) the characteristics of the saddle dolomite (D4), Well Bg22 2233.04 m, Ordovician formation, plane-polarized light; (l) characteristics of cathode luminescence of the saddle dolomites (D4) in the same field of view as k, CL. CL is a cathode luminescence characteristic.

4.1.5. Fine-Crystalline Ferroan Dolomite Cements (D2)

Fine-crystalline ferroan dolomite cements mainly filled in the fractures. It can be inferred that the fine-crystalline ferroan dolomite cement was formed after the stylolite (Figure 3g,h). This kind of dolomite cement is dyed blue by alizarin red mixed with potassium ferric hydroxide (Figure 3g–i). The crystal size of the ferroan dolomite depends on the fracture scale. In general, fractures with a width less than 0.25 cm are highly likely to be filled with fine-crystalline ferroan dolomite cements (D2). This type of dolomite cement commonly has a weak dull red color under CL (Figure 4f).

4.1.6. Medium-to-Coarse-Crystalline Dolomite Cements (D3)

Medium-to-coarse-crystalline dolomite cements consist of 250 μm to 500 μm crystals, with some being larger than 500 μm . The dolomite crystals mostly display a planar texture (Figure 5b,c,e,f). This type of dolomite cement fills in dissolution or structure fractures

(Figure 5a,d). The dolomite crystals were partially dissolved by late organic acid fluid, forming dissolution pores (Figure 5b,c,e). This type of dolomite is mainly present in the Cambrian strata and in smaller amounts in the Ordovician strata. The medium-to-coarse-crystalline dolomite cements have red cathodoluminescence characteristics, with obvious luminous bands in the dolomite crystals (Figure 5h–j)

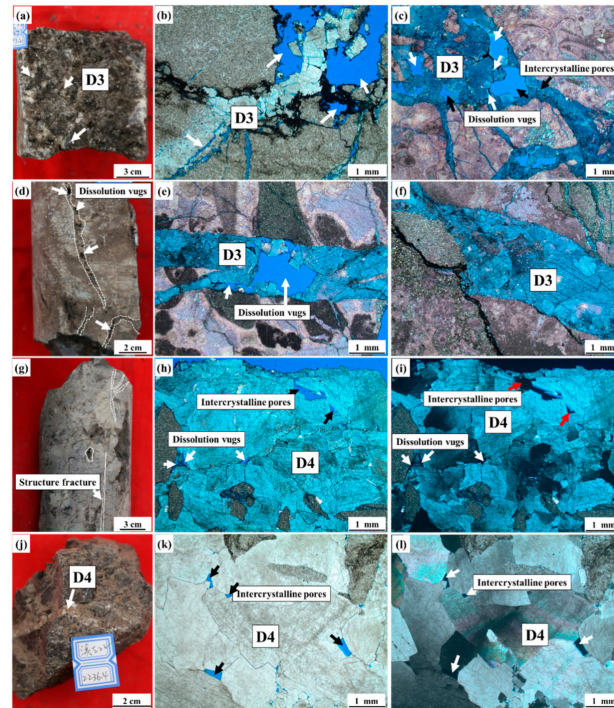


Figure 5. Petrological characteristics of the medium-to-coarse-crystalline dolomite cements (D3) and saddle dolomite (D4). (a) The medium-to-coarse-crystalline dolomite cements (D3) filled in the vertical fractures, and there is an obvious hydrocarbon charging phenomenon, Well Bg26 2793.2 m, Zhangxia formation, core; (b) microcrystalline dolomite; the developed dissolution fractures are filled in with medium-to-coarse-crystalline dolomite cements. The hydrocarbon dissolved the dolomite crystals and formed the dissolution vugs, shown by the white arrow, Well Bg22 2246.89 m, Ordovician formation, plane-polarized light; (c) bioclastic limestone; the medium-to-coarse-crystalline dolomite cements are filled in the structure fracture and formed the intercrystalline pores, shown by the black arrow. Some of the dolomite crystals were dissolved by the hydrocarbon and formed the dissolution vugs, shown by white arrow, Well Bg26 2793.2 m, Zhangxia formation, plane-polarized light; (d) the vertical fracture dissolved by the fluid and formed the dissolution vugs (shown by the white arrow), which are filled by coarse dolomite crystals, Well Bg26 2795.1 m, Zhangxia formation, core; (e) bioclastic limestone; structure fracture is developed and is filled in with medium-to-coarse-crystalline dolomite cements. Additionally, dolomite crystals are dissolved by fluid, forming the dissolution vugs (shown by white arrow), Well Bg26 2795.4 m, Zhangxia formation, plane-polarized light; (f) bioclastic limestone; medium-to-coarse-crystalline dolomite cements are tightly filled in the dissolution fractures. The dolomite crystals at the edge of the fracture are mainly medium-crystalline dolomite cements, while the size of the dolomite crystals at the center of the fracture increases gradually, Well Bg26 2798.2 m, Zhangxia formation, plane-polarized light; (g) microcrystalline dolomite; structural fractures developed, Well Bg22 2211.17 m, Ordovician formation, core; (h) microcrystalline dolomite; saddle dolomites are filled in the fracture, Well Bg22 2211.17 m, Ordovician formation, plane-polarized light; (i) saddle dolomites in the same view as h, perpendicular polarized light; (j) microcrystalline dolomite; high-angle structural fractures are filled by the saddle dolomites, Well Bg22 2236.4 m, Ordovician formation, core; (k) microcrystalline dolomite; characteristic of saddle dolomites are filled in fractures, and intercrystalline pores are formed by saddle dolomite crystals (the black arrow), Well Bg22 2246.89 m, Ordovician formation, plane-polarized light; (l) saddle dolomite in the same view as k, perpendicular polarized light.

4.1.7. Saddle Dolomite (D4)

Saddle dolomites are coarse crystalline, are much larger than 500 μm , and exhibit curved crystal faces. Under perpendicular polarized light, the saddle dolomites show wavy extinction (Figure 5i,l). Small-scale intercrystalline pores are developed between the saddle dolomites (Figure 5h,k). Parts of the edge of the saddle dolomites are dissolved and form the dissolution vugs (Figure 5h). Saddle dolomite has been observed in fractures (Figure 5g,j) and is mainly present in pores or cavities in the Ordovician strata. Previous studies have shown that the saddle dolomite is related to fractures and is possibly due to hydrothermal events [31,50].

4.2. Dolomite Reservoir Characteristics

There are various reservoir spaces in the dolomite reservoir of the Lower Paleozoic strata in the Dongying Depression. Reservoir spaces can be divided into pores and fractures according to the observations of the cores and thin sections.

4.2.1. Pore

The pores types include moldic pores, intercrystalline pores, and dissolution vugs.

Moldic Pore

Moldic pores are formed by the selective dissolution of early calcite or gypsum cements by meteoric water [51], and the morphology of the dissolved particles is retained. The pore diameter (long axis) of the moldic pores in the study area is between 211 μm and 655 μm (Figure 2d).

Intercrystalline Pore

Intercrystalline pores occupy a large proportion of all types of reservoir space. These intercrystalline pores are between mineral crystals [52]. Dolomite crystals with different structures form intercrystalline pores of different sizes. The powder-to-fine-crystalline dolomite cements (D1) mainly form micro intercrystalline pores (Figure 3e). Saddle dolomite (D4) overgrowth also forms small-scale intercrystalline pores (average size 288 μm) (Figure 4h,i,k,l and Figure 6a). Medium-to-coarse-crystalline dolomite cement (D3) tends to form relatively large intercrystalline pores (Figures 4c and 6b).

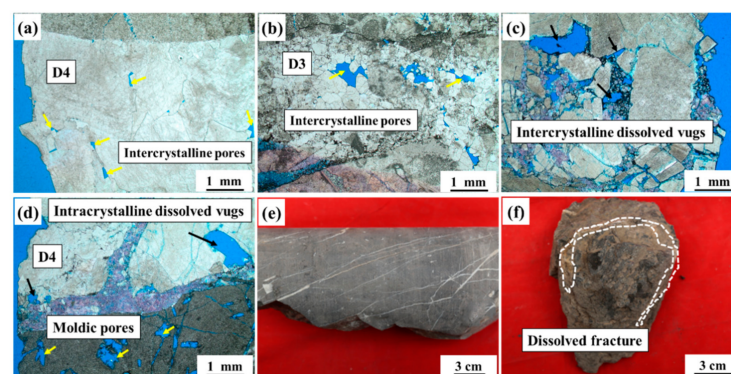


Figure 6. The reservoir space characteristics of the dolomite reservoir in the Dongying Depression, Bohai Bay Basin. (a) The intercrystalline pores (yellow arrow) between the saddle dolomites (D4), Well Bg22 2246.89 m, Ordovician formation, plane-polarized light; (b) the intercrystalline pores (yellow arrow) between the medium-to-coarse-crystalline dolomite cements, Well Bg26 2793.2 m, Zhangxia formation, plane-polarized light; (c) intercrystalline-dissolved vugs (black arrow) between the saddle dolomites (D4), Well Bg22 2236.4 m, Ordovician formation, plane-polarized light; (d) intracrystalline dissolved vugs (black arrow) within the saddle dolomites (D4), Well Bg22 2233.04 m, Ordovician formation, plane-polarized light; (e) microcrystalline dolomite (M2) high-angle structural fractures, Well Bg22 2348.4 m, Ordovician formation, core; (f) microcrystalline dolomite (M2), dissolved fractures (white dotted line), the saddle dolomites fill in the fracture, Well Bg22 2235.84 m, Ordovician formation, core.

Dissolution Vugs

Dissolution vugs include intercrystalline-dissolved vugs and intracrystalline-dissolved vugs. Dolomite were dissolved and enlarged by supergene and late diagenetic dissolution, forming enlarged dissolution pores [53]. Dissolution vugs commonly have harbor shapes. The dissolution fluids are mainly composed of hydrothermal fluid and/or organic acid fluid. Black bitumen can be seen in or around the edge of the dissolution vugs.

4.2.2. Fracture

Fractures can be divided into structural fractures and dissolution fractures according to their genesis [54,55]. Tectonic stress promotes the formation of structural fractures, including low-angle fractures, oblique fractures, and high-angle fractures, which are relatively straight (Figure 6e). Since then, diagenetic fluids have mainly dissolved (expand) the structural fractures or unstable rocks, causing the fracture edge to be curved and smooth. Hydrothermal minerals and black residual bitumen filled within the dissolution fractures, indicating that the dissolution fluid may be hydrothermal fluid or organic acid fluid (Figures 4b and 6f).

4.3. Isotope Data

4.3.1. Stable Isotopes

The results of the O isotope VPDB and C-isotope VPDB values are presented in Figure 7. The argillaceous dolomites (M1) have $\delta^{18}\text{O}$ VPDB values of about -6‰ , and the $\delta^{18}\text{O}$ values of the microcrystalline dolomite (M2) range from -9.3‰ to -6.2‰ . The fine-crystalline dolomite (M3) has $\delta^{18}\text{O}$ values of about -9.3‰ . The dolomite cements filling in the fractures or dissolution vugs have more negative $\delta^{18}\text{O}$ values than the matrix dolomites do. The $\delta^{18}\text{O}$ values of the powder-to-fine-crystalline dolomite cements (D1) range from -10‰ to -5.2‰ , the $\delta^{18}\text{O}$ value of the fine-crystalline ferroan dolomite cements (D2) is -14.1‰ . The $\delta^{18}\text{O}$ values of the medium-to-coarse-crystalline dolomite cements (D3) range from -15.7‰ to -12.7‰ . The saddle dolomites have more negative $\delta^{18}\text{O}$ values than other types of the dolomite in the study areas, ranging from -25.7‰ to -23.7‰ . The $\delta^{13}\text{C}$ values of the dolomites range from -1.9‰ to 0.5‰ .

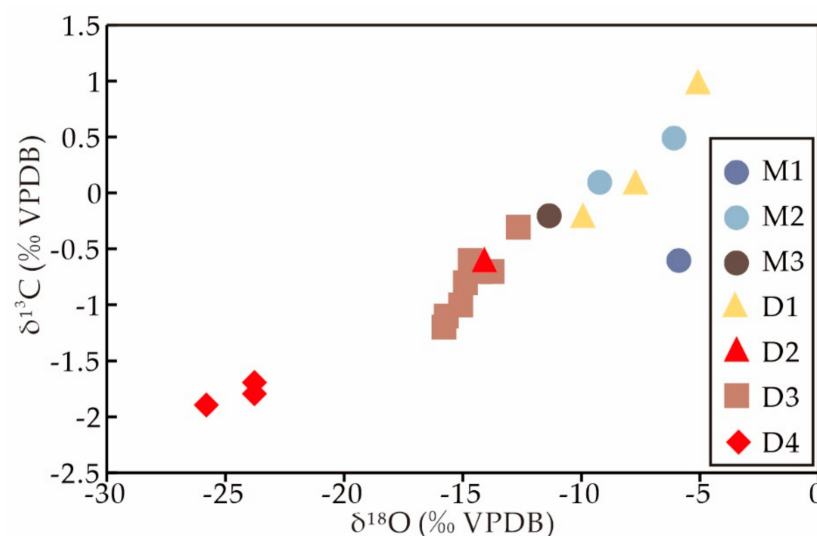


Figure 7. Stable isotope values for the dolomites of the Lower Paleozoic strata in the Dongying Depression, Bohai Bay Basin. M1: argillaceous dolomite; M2: microcrystalline dolomite; M3: fine-crystalline dolomite; D1: powder-to-fine-crystalline dolomite cement; D2: fine-crystalline ferroan dolomite cement; D3: medium-to-coarse-crystalline dolomite cement; D4: saddle dolomite.

4.3.2. Strontium Isotope

The Sr isotope ratios of the dolomites are displayed in Figure 8. The microcrystalline dolomite (M2) $^{87}\text{Sr}/^{86}\text{Sr}$ ratio is about 0.7091, within the range of the Latest Cambrian to Middle Ordovician seawater [56,57]. The $^{87}\text{Sr}/^{86}\text{Sr}$ ratio of the powder-to-fine-crystalline dolomite cements (D1), fine-crystalline ferroan dolomite cements (D2), and the medium-to-coarse-crystalline dolomite cements (D3) range from 0.7119 to 0.7129, which are higher than those of the microcrystalline dolomite. The $^{87}\text{Sr}/^{86}\text{Sr}$ ratio of the saddle dolomite (D4) has a wide range, from 0.7093 to 0.7112.

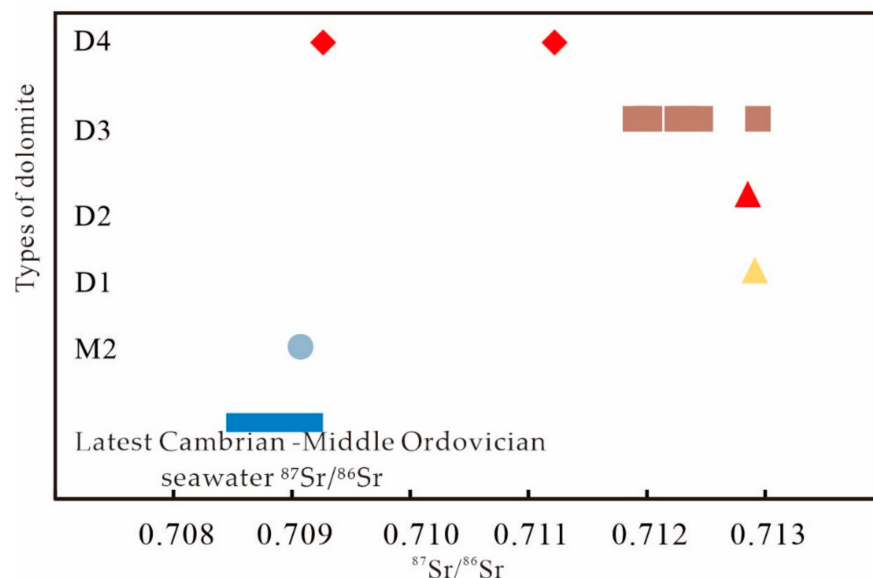


Figure 8. Comparison of radiogenic strontium isotope ratios between Lower Paleozoic dolomite and Latest Cambrian to Middle Ordovician seawater. The $^{87}\text{Sr}/^{86}\text{Sr}$ ratios of Latest Cambrian to Middle Ordovician seawater from [56,57]. M2: microcrystalline dolomite; D2: fine-crystalline ferroan dolomite cements; D3: medium-to-coarse-crystalline dolomite cements; D4: saddle dolomite.

5. Discussion

5.1. Diagenesis of the Dolomite Reservoir

Carbonate rocks may undergo a variety of diagenesis mechanisms after deposition, changing the physical properties of carbonate reservoirs. According to the thin sections and core study, the dolomite reservoirs in the study areas mainly experienced six types of diagenesis: dolomitization, dissolution, fracturing, cementation, compaction, and pressure solution.

5.1.1. Dolomitization

Dolomitization is widely developed in the limestone at the bottom of the Ordovician formation and the oolitic limestone in the Cambrian formation. The $^{87}\text{Sr}/^{86}\text{Sr}$ ratios of the fine-crystalline dolomite cements have similar $^{87}\text{Sr}/^{86}\text{Sr}$ ratio values to those of argillaceous dolomite (M1) and microcrystalline dolomite (M2), and the Latest Cambrian to Middle Ordovician seawater [56,57]. D1 are associated with stylolite and anhydrite. These characteristics indicate that powder-to-fine-crystalline dolomite cements (D1) may have been formed by the evaporation and condensation of Cambrian–Ordovician seawater in the early stage.

5.1.2. Dissolution

In the area around where dissolution occurs, the residual black bitumen can be seen around the edges of the dolomite crystals and in some dissolution fractures (Figure 5b) and dissolution vugs (Figure 6c), indicating the charging of the organic matter fluid. The

margin of the dissolution fracture is not straight and is an embay in shape, and the local enlargement of the fractures appeared (Figure 5c). Pyrite, saddle dolomite, quartz, and other hydrothermal minerals have been observed in the dolomite reservoirs, indicating hydrothermal fluid activity. Additionally, these hydrothermal minerals are accompanied by dissolution pores (Figure 9a). This evidence indicates that organic acid fluids and hydrothermal fluids are the main dissolution fluids for the dolomite, leading to the dissolution of dolomite and the formation of dissolution fractures or dissolution vugs.

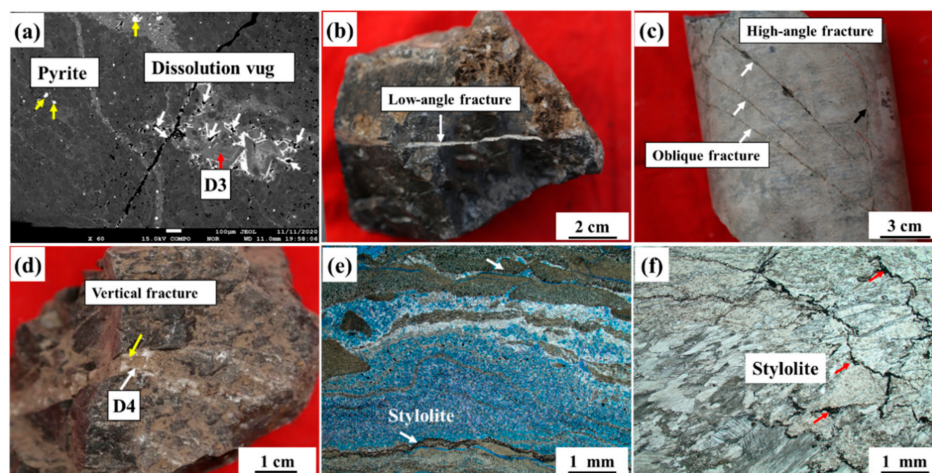


Figure 9. Diagenesis types of dolomite reservoirs in the Dongying Depression, Bohai Bay Basin. (a) Microcrystalline dolomite; hydrothermal dissolution vugs. The pyrite filled in the vugs (yellow arrow), and medium-to-coarse-crystalline dolomite cement was dissolved and formed intragranular dissolution pores, Well Bg22 2246.89 m, Ordovician formation, backscattered image; (b) microcrystalline dolomite; low-angle fracture, filled with calcite cements; Well Bg26 2515.2 m, Yeli-Liangjiashan formation, core; (c) oblique fractures (white arrow) formed before high-angle fractures (black arrow), Well Bg26 2803.7 m, Zhangxia formation, core; (d) microcrystalline dolomite; vertical fracture (yellow arrow), filled with saddle dolomite; Well Bg22 2236.4 m, Ordovician formation, core; (e) the stylolite (white arrow) was formed by compaction and pressure solution, and filled argillaceous material; Well Bg22 2219.27 m, Ordovician formation, thin section; (f) the stylolite (red arrow) formed by compaction and pressure solution, and filled with organic matter; Well Bg22 2348.95 m, Ordovician formation, thin section. D3: medium-to-coarse-crystalline dolomite cements; D4: saddle dolomite.

5.1.3. Fracturing and Cementation

Tectonic stresses cause rocks to fracture and can form a series of fractures. The main types of fractures include low-angle fractures, high-angle fractures, and vertical fractures. The sequence of fractures can be distinguished according to the intersecting relationships between fractures. In the early stages, low-angle fractures and oblique fractures were mainly formed and were filled by the calcite cements (Figure 9b,c). In the late stages, high-angle fractures and vertical fractures were formed and were filled by the medium-to-coarse-crystalline dolomite cements (D3) and saddle dolomites (D4) (Figure 9d).

5.1.4. Compaction and Pressure Solution

A large number of stylolites were found in the study area, indicating that the reservoir underwent strong compaction and pressure solution (Figure 9e,f).

5.2. Origins of the Different Types of Dolomite

5.2.1. Matrix Dolomites

Matrix dolomites mainly include argillaceous dolomite (M1), microcrystalline dolomites (M2), and fine-crystalline dolomites (M3) from the restricted and tidal flat face and tend to be mainly microcrystalline to fine crystals with a euhedral–subhedral crystal texture. M1 and M2 have the smallest crystal size. This indicates that M1 and M2 grow during

the early stages of diagenesis [58]. The $\delta^{13}\text{C}$ values of the matrix dolomites (0.5~−1‰, VPDB) are similar to those of contemporaneous limestone (−1.5~−1.1‰). The $\delta^{18}\text{O}$ values of M1 and M2 range from −9.3 to −6‰ VPDB. Using the dolomite–water oxygen isotope fractionation equation $1000\text{Ln}\alpha_{(\text{dolomite-water})} = 3.14 \times 10^6\text{T}^{-2} - 2.0$ proposed by Land [59], and assuming a temperature of 25 °C, the $\delta^{18}\text{O}$ values of the water present during the growth of M1 and M2 were calculated. The results of the calculations show that the $\delta^{18}\text{O}$ values of the water present during the growth of M1 and M2 ranged from −12.1 to −8‰ VSMOW. The $\delta^{18}\text{O}$ values of the brachiopods from the Cambrian–Ordovician strata commonly range from −10 to −3‰ VPDB [60]. Using the calcite–water oxygen isotope fractionation equation $1000\text{Ln}\alpha_{(\text{calcite-water})} = 2.78 \times 10^6\text{T}^{-2} - 2.89$ proposed by Friedman and O’Neil [61], the $\delta^{18}\text{O}$ values of seawater during the growth of brachiopods were calculated. The $\delta^{18}\text{O}$ values of the seawater during brachiopod growth are between −9.2 and −2.1‰ VSMOW (Figure 10). It can be seen that the $\delta^{18}\text{O}$ values of the argillaceous dolomite (M1) and microcrystalline dolomite (M2) were more negative than the $\delta^{18}\text{O}$ value of the Cambrian–Ordovician seawater (−9.2 to −2.1‰, VSMOW). However, the $^{87}\text{Sr}/^{86}\text{Sr}$ ratio of microcrystalline dolomite (M2) is about 0.7091, falling within the $^{87}\text{Sr}/^{86}\text{Sr}$ range of Latest Cambrian to Middle Ordovician seawater. These indicate that seawater may be the main diagenetic fluid for M1 and M2 formation. M1 and M2 have more negative $\delta^{18}\text{O}$ values than that of seawater and are likely to be affected by the hydrothermal fluid or meteoric water. Fine-crystalline dolomite (M3) have a larger crystal size than M1 and M2, indicating that M3 were formed relatively later than M1 and M2. Moreover, early diagenetic gypsum (now transformed to anhydrite) is present in the dolomite strata. This supports sabkha capillary zone dolomitization [62,63] and reflux dolomitization models [64]. Anhydrite cements have been observed in the formation where M3 are developed in the study area. Additionally, the main sedimentary environments in the study area are the gypsum dolomite flat with strong evaporation and supratidal–intertidal flat during the deposition period of Majiagou formation [65]. Therefore, M3 could have been formed by the seepage reflux of seawater in an evaporative environment.

5.2.2. Powder-to-Fine-Crystalline Dolomite Cements (D1)

Power-to-fine-crystalline cements (D1) are commonly planar rhombic textures, indicating that D1 were formed at relatively low temperatures during the early shallow burial stage [66]. D1 are distributed along the stylolite in limestone samples, indicating that the formation of D1 is related to stylolite. D2 is generally distributed on both sides of the stylolite. Some dolomites are dissolved and have uneven crystal edges (Figure 3b,c). Some studies have reported that the dissolution of the limestone along the stylolite may accelerate dolomitization through the flow of Mg-rich fluids [67]. Therefore, the powder-to-fine-crystalline dolomite cements associated with stylolite may be formed at the same time as or after stylolite. Stylolite was formed by the chemical compaction and is of various scales and sizes. Some scholars have considered that pressure dissolution can occur at the depth of 610~914 m, forming stylolite [68], and can also occur at the deep burial environment [69]. In recent years, pioneers have proposed that stylolite forms at a depth of between 500 m and 1 km [70]. According to the burial history in the study areas. D1 may have been formed by metasomatic calcite from lower Ordovician dolomites. The $\delta^{18}\text{O}$ values of the powder-to-fine-crystalline dolomite cements (D1) ranged from −5.2‰ to −10‰ (VPDB). Using the dolomite–water oxygen isotope fractionation equation proposed by Land $1000\text{Ln}\alpha_{(\text{dolomite-water})} = 3.14 \times 10^6\text{T}^{-2} - 2.0$, the $\delta^{18}\text{O}$ values of fluid forming dolomite precipitates were calculated. The calculation results show that the $\delta^{18}\text{O}$ values of the fluid-forming dolomite precipitates are between −8 and −3.8‰ VSMOW. The $\delta^{18}\text{O}$ values of fluid forming dolomite precipitates are similar to the oxygen isotope values of the Paleozoic seawater (−9.2 to −2.1‰, VSMOW) [71]. This suggests that seawater is the main dolomitic fluid. However, Figure 8 shows that the $^{87}\text{Sr}/^{86}\text{Sr}$ ratio of the D1 dolomite is greater than that of the Latest Cambrian to Middle Ordovician seawater, further indicating that D1 may be influenced by the continental formation of water rich in radioactive Sr in

the shallow burial environment [72]. In some samples, unstable calcite carbonate filled in ooids replaced by D1 (Figure 3f). Calcite that filled in the ooids is dissolved to form moldic pores, the dolomitizing fluid then enters the moldic pores. When the fluid is highly saturated, recrystallization development occurs to form the powder-to-fine-crystalline dolomite cements (D1) [58,66]. Sparry calcite cements developed in the intercrystalline pores (Figure 3f), suggesting that the powder-to-fine-crystalline dolomite cements were formed relatively early in diagenetic history.

5.2.3. Fine-Crystalline Ferroan Dolomite Cements (D2) and Medium-to-Coarse-Crystalline Dolomite Cements (D3)

D2 and D3 dolomite cements have a larger crystal size than D1 dolomite cements, indicating that D2 and D3 dolomite cements are formed in higher-temperature conditions [58,73]. The most obvious difference between the D2 and (D3) dolomite cements and D1 dolomite cements is that the D2 and D3 dolomite cements are stained blue and exhibit the ferroan dolomite cement characteristics under the microscope. The iron-rich dolomite is the result of hydrothermal fluids action in a deep burial environment [74,75]. Dolomite crystals have obvious cathodoluminescence bands, suggesting that the D2 and D3 dolomite cements have multi-stage recrystallization [76]. The D2 and D3 dolomite cements filled in the fractures. Previous studies have analyzed the carbon and oxygen isotopes of calcite filling in high-angle fractures formed in the Yanshan period and found $\delta^{18}\text{O}$ values between -19‰ and -15‰ VPDB, $\delta^{13}\text{C}$ values between -0.5‰ and -3.0‰ VPDB [77], and the fluid inclusions homogenization temperatures are between 120 °C and 150 °C . Using the calcite–water oxygen isotope fractionation equation $1000\text{Ln}\alpha_{(\text{calcite-water})} = 2.78 \times 10^6\text{T}^{-2} - 2.89$ proposed by Friedman and O’Neil [61], the $\delta^{18}\text{O}$ values of fluid-forming calcite precipitates were calculated. The $\delta^{18}\text{O}$ values of fluid forming calcite precipitates ranged from -1.4 to 0.18‰ VSMOW. The $\delta^{18}\text{O}$ values of D2 and D3 ranged from -15.8 to -12.7‰ VPDB. Using the ferroan dolomite–water oxygen isotope fractionation equation $1000\text{Ln}\alpha_{(\text{dolomite-water})} = 2.78 \times 10^6\text{T}^{-2} + 0.11$ proposed by Fisher and Land [78], the $\delta^{18}\text{O}$ values of fluid forming D2 and D3 precipitates were calculated (Figure 10). The results show that the $\delta^{18}\text{O}$ values of fluid forming D2 and D3 precipitates are between -1.4‰ and 0.2‰ VSMOW. This result shows a high degree of overlap with the $\delta^{18}\text{O}$ values of the diagenetic fluids from the calcite in the Yanshan veins in the study area, indicating that the diagenetic fluid of D2 and D3 is likely to be similar to the vein calcite cements formed during the Yanshan period. The calcite cement and D2, and D3 in the veins, were formed from precipitation from hydrothermal fluids during the Yanshan period. The crust was folded and uplifted, and the platform was activated, forming a series of fault depressions and uplifting the fault blocks during the Late Triassic–Early Jurassic periods, forming the fracture systems [79]. The Yanshan Movement, which began at the end of the Early Jurassic period, was the initial stage of volcanic activity in the Bohai Bay Basin [80,81]. In particular, the second act of the Yanshan Movement was characterized by intense magmatic activity accompanied by intense faulting [82], providing a sufficient heat source and Fe^{2+} for iron-rich dolomite cements. Furthermore, the homogenization temperatures of fluid inclusions, which were shown to range in temperature from 120 to 181 °C , are higher than the maximum burial temperature (140 °C) in the study area [83], suggesting that D2 and D3 may be formed by hydrothermal fluid. D2 and D3 dolomite cements have higher $^{87}\text{Sr}/^{86}\text{Sr}$ ratios (0.7119 to 0.7129) than Cambrian–Ordovician seawater (Figure 8) and are close to the crust source of hydrothermal fluids [84]. A higher $^{87}\text{Sr}/^{86}\text{Sr}$ ratio indicates that ^{87}Sr -enriched fluids were involved in the diagenesis of the dolomite. ^{87}Sr -enriched fluid may derive from the fluid formed by the eroding of siliciclastic sediments containing argillaceous and/or feldspathic components. The Maozhuang and Xuzhuang formations are deposited with shale and sandstone with a total thickness of about 200 m . When the sandstone is dominated by feldspar, migrating hydrothermal fluids may be able to acquire radioactive Sr isotope. Therefore, D2 and D3 have the characteristics of a high temperature of hydrothermal fluid and high $^{87}\text{Sr}/^{86}\text{Sr}$ ratio of crust source.

5.2.4. Saddle Dolomite (D4)

Saddle dolomites in the Ordovician formation are filled with high-angle fractures, have largest crystals, curved crystal faces, and wavy extinction characteristics, suggesting that D4 may have been formed by the rapid precipitation of high temperatures of Mg-rich fluids during late diagenesis [17,63]. Previous studies and the high homogenization temperature of the inclusions (>200 °C) have indicated that D4 was formed by hydrothermal fluids.

The $\delta^{18}\text{O}$ values of dolomite can reflect the environmental conditions and temperature during the formation and diagenesis of carbonate rocks [85,86]. Saddle dolomites (D4) show that the $\delta^{18}\text{O}$ values (−23.7 to −25.7‰ VPDB) are more negative than other types of the dolomite cements (Figure 7). Utilizing the formula $10^3\text{Ln}\alpha_{(\text{dolomite-water})} = 3.14 \times 10^6\text{T}^{-2} - 2.0$ proposed by Land [59], the $\delta^{18}\text{O}$ of the water present during the growth of D4 was between −6.7‰ and −5.0‰ VSMOW. The $\delta^{18}\text{O}$ values of the D4 are more negative compared to the $\delta^{18}\text{O}$ VSMOW values of the magmatic water (Figure 10). Additionally, this result is more negative than that of common hydrothermal saddle dolomites. The $\delta^{18}\text{O}$ value of D4 fluid is significantly lower than that of normal saddle dolomite, which may be caused by the following reasons: (1) The $\delta^{18}\text{O}$ values of the dolomite are controlled by temperature. As the temperature increases, ^{18}O are depleted, Therefore, dolomite has a lower $\delta^{18}\text{O}$. The homogenization temperature of the saddle dolomite inclusions in the lower Paleozoic in the southwest of the Dongying Depression is more than 200 °C (Figure 10), which is higher than that of common saddle dolomite inclusions (100~180 °C) [17,87]; (2) there may be ^{18}O depleted hydrothermal fluids injection during diagenesis. The host dolomites can be dissolved by the hydrothermal fluids. Saddle dolomites are mainly developed in the Ordovician microcrystalline dolomite strata. The main sedimentary environment of the Majiagou period is gypsum dolomite flat with strong evaporation and supratidal–intertidal flat in the study area [65]. The evaporation phase is enriched with light oxygen, so the host dolomites also have low $\delta^{18}\text{O}$ values. When the host dolomites with low $\delta^{18}\text{O}$ values were dissolved by hydrothermal fluids with low $\delta^{18}\text{O}$ values, saddle dolomite may have had extremely negative $\delta^{18}\text{O}$ values. The $^{87}\text{Sr}/^{86}\text{Sr}$ ratios of some host dolomites are similar to that of saddle dolomite. Which also supports this inference.

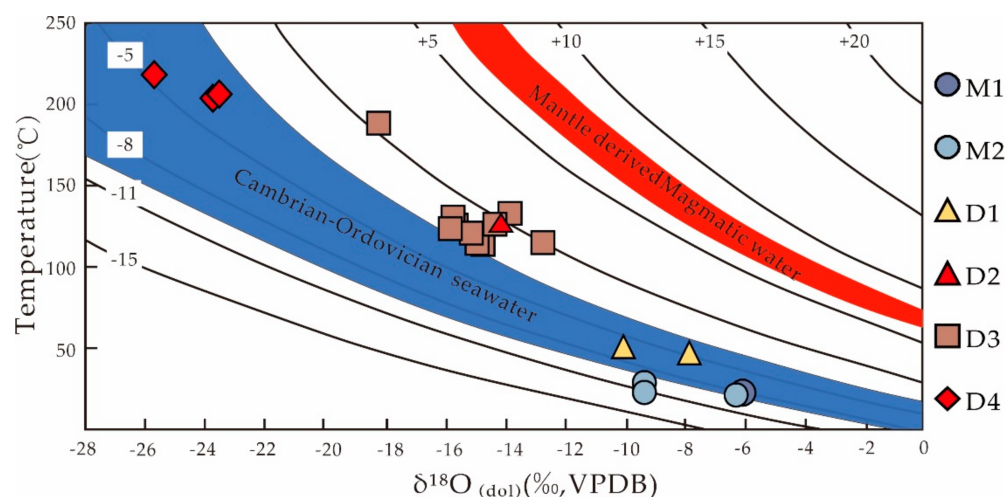


Figure 10. Crossplots of fluid inclusion homogenization temperature (Th) against oxygen signature for the matrix dolomite and various dolomite cements in the southwest of the Dongying Depression, Bohai Bay Basin. The data for mantle-derived magmatic water are quoted from [88]. M1: argillaceous dolomite; M2: microcrystalline dolomite; D1: powder-to-fine-crystalline dolomite cements; D2: fine-crystalline ferroan dolomite cements; D3: medium-to-coarse-crystalline dolomite cements; D4: saddle dolomite.

5.3. Implications for Porosity Development

5.3.1. Diagenetic Pore Evolution

On the basis of petrological observation, this study identified the diagenesis and diagenetic sequence of the reservoir and summarized the diagenetic pore evolution model of the reservoir (Figure 11).

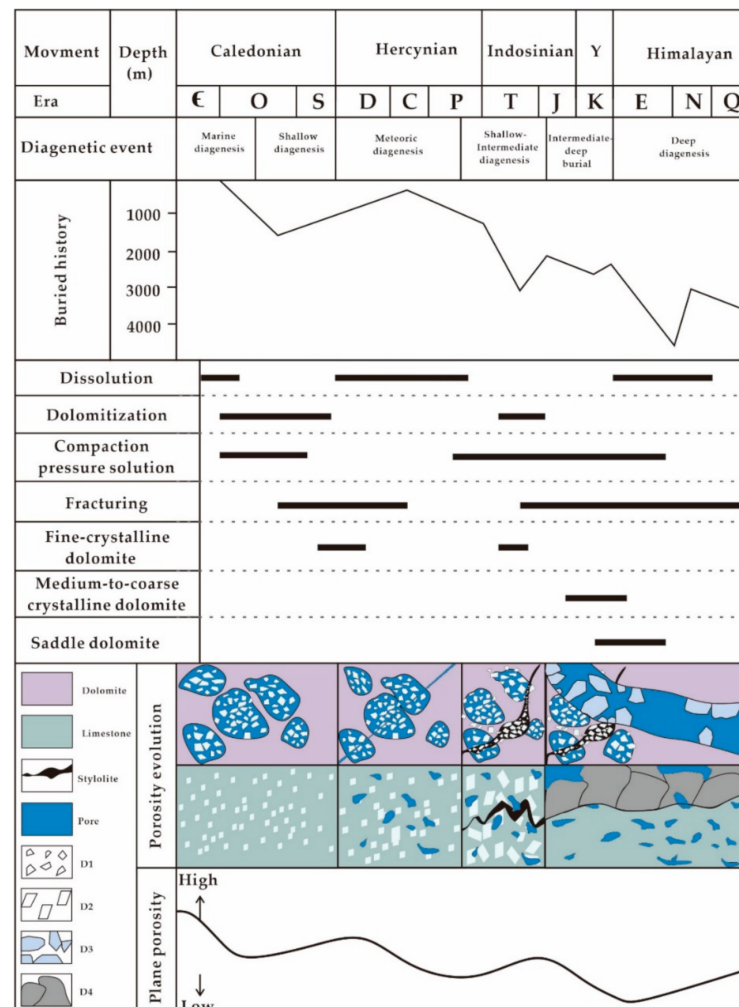


Figure 11. Diagenetic events and pore evolution of dolomite reservoir of the Lower Paleozoic strata in the Dongying Depression, Bohai Bay basin. Y represents Yanshan movement; D1: powder-to-fine-crystalline dolomite cements; D2: fine-crystalline dolomite cements; D3: medium-to-coarse-crystalline dolomite cements; D4: saddle dolomite.

In the early diagenetic stage, early calcite cements filled in the space between grains (oolites or rubble), reducing the primary porosity. The Cambrian–Ordovician strata were uplifted and affected by Caledonian movement [89], and the oolites were selectively dissolved by diagenetic fluids and formed moldic pores. At the moment, the powder-to-fine-crystalline dolomite cements (D1) formed by the seepage reflux mechanism are cemented in residual oolites. However, the plane porosity produced by the powder-to-fine-crystalline dolomite cements (D1) are commonly lower than 0.1%. Dolomitization at the early diagenesis is not the main diagenesis to increase the porosity. With the increase in the buried depth, the strata enters the subsidence stage, and pore reduction such as compaction occurs. Compaction reduces rock volume, dissolves grains, and decreases the proportion of intercrystalline pores, leading to a sharp decrease in porosity [90].

5.3.2. The Influence of Diagenesis on Reservoir Properties

Studies have shown that the fracture system, dissolution, and cementation play important roles in the formation of reservoir spaces [17,32,91,92]. The plane porosity of the rocks can reach 48% in the early stages of fracture formation. After the fault system is formed, hydrothermal fluids along with the fractures move upward, the matrix dolomite dissolves, and dissolution vugs and dissolution fractures begin to form. The saturability of the fluid changes as the fluids react with the host rocks. Subsequently, D3 and D4 dolomite cements begin to form during the intermediate-deep burial diagenesis. The D3 and D4 dolomite cements are fully filled in (or semi-filled in) the fractures. This cementation process causes serious damage to the previously formed fracture reservoir system [93]. After cementation, the plane porosity of the rocks is only 6% and can be even less than 1%. The residual pores after cementation are the main sites of late organic acid dissolution.

Petrological observations reveal high-temperature dolomite cements, pyrite, and secondary dissolution (irregular edges of pores and fractures), and the residual bitumen observed in the interior of the dissolution pores and fractures. In summary, the study area is extensively influenced by hydrothermal fluids and organic acids.

Fluid migration is controlled by faults [17,87,94]. The more developed the fault, the more obvious the fluid action. Dissolution is the main diagenesis to form effective reservoir spaces in the study area [40,95]. A series of needle-like dissolution vugs are formed as hydrothermal fluids migrate up the fractures and faults [91]. Dissolution is the key factor to form high-quality reservoirs. Due to the striking volcanic activity, hydrothermal dissolution is a main dissolution process during the intermediate-to-deep burial stages. When the reservoir is closer to the intrusions and faults, the dissolution phenomenon is more obvious, and more dense dissolution vugs are developed. The reservoir shows good productivity. Since the dissolution and precipitation of the hydrothermal fluid are usually accompanied and since fluid saturation increases, hydrothermal dissolution gradually turns into hydrothermal precipitation [16]. The cements formed by hydrothermal precipitation fill the fractures.

In general, the plane porosity of saddle dolomite is lower than that of medium-to-coarse-crystalline dolomite (Figure 12), which may be due to the joint influence of the crystal structure and mineral filling degree of the fractures. Saddle dolomite has larger crystals than medium-to-coarse-crystalline dolomite, and the fractures are usually fully filled in with saddle dolomite. Therefore, the rock is less affected by fluid dissolution, and the plane porosity of the rock is relatively low (Figure 12a,b). Medium-to-coarse-crystalline dolomite partially fills in fractures, and fractures with high residual pores. Additionally, the rocks that developed medium-to-coarse-crystalline dolomite have a higher degree of dissolution than the rocks that developed saddle dolomite (Figure 12). Magmatic activity mainly developed during the Yanshan movement, and some magmatic activity developed during the late Triassic period [79,96,97]. Residual bitumen is commonly filled between dolomite cements formed by high-temperature fluids. The oil and gas charging period represent the sedimentary period of the Shahejie Formation [98]. All of this evidence indicates that the dissolution of organic acids occurs after hydrothermal dissolution. Therefore, the dissolution vugs that are formed by organic acid dissolution can be better preserved [99]. Organic acid dissolution can form higher plane porosity than hydrothermal dissolution according to other plane porosity statistics (Figure 12). Additionally, the reservoirs are closer to the source layer or basin and the dissolution of organic acids is more intense.

Dolomite is more likely to form effective fractures than limestone due to its greater mechanical strength [100,101]. Thus, dolomite reservoirs are more likely to form high-density fractures as well as fractured reservoir systems. Additionally, the closer the formations and wells are to the fault plane, the higher the density of the structural fractures according to the statistic of the cores and thin sections (Figure 13). These fractures are interconnected to form a large fractured reservoir system, which plays a constructive role in reservoir reconstruction. The rocks with a high fracture density and low fracture filling degree are often subjected to more intense dissolution, and the rocks have higher plane porosity

(Figure 12c). On the contrary, the dissolution of rocks is not obvious and the plane porosity percentage is relatively low (Figure 12d).

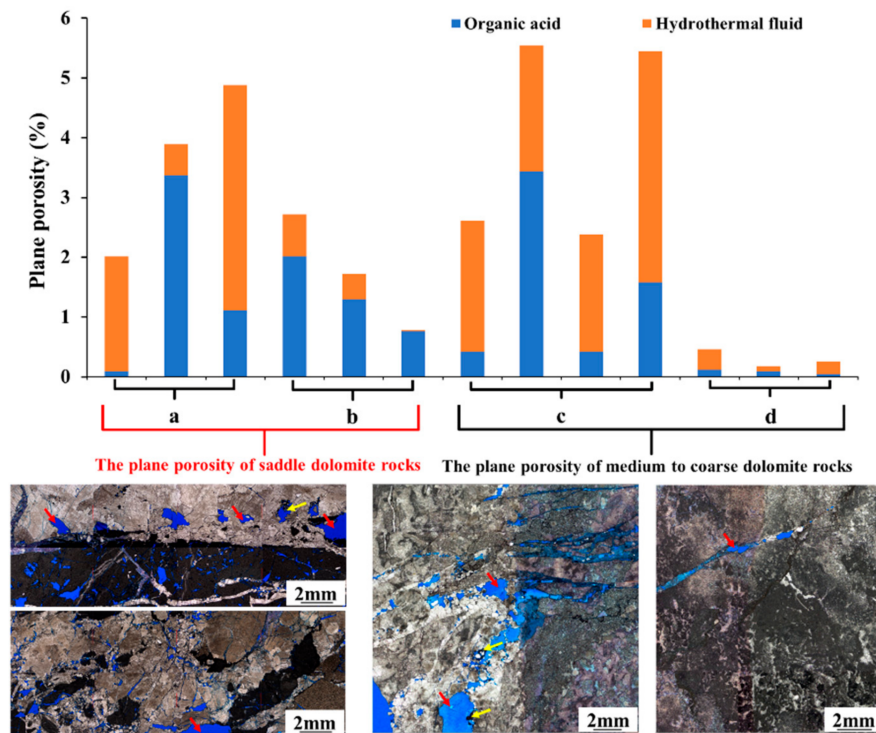


Figure 12. The total plane porosity of all kinds of dolomite cements with different textures and the rate of contribution of different fluids to the percent of area pores. (a) The contribution of dissolution to the plane porosity of the rocks that developed saddle dolomite and its microscopic characteristics when dissolution is strong; (b) when the dissolution is not obvious, the contribution of dissolution to the plane porosity of the rocks developed saddle dolomite and its microscopic characteristics; (c) the rock developed with a high-density fracture area, and the image shows the contribution of dissolution to the plane porosity of the rocks; (d) the rock developed a low-density fracture area, and the image shows the contribution of dissolution to the plane porosity of the rocks; red arrow: dissolution vugs; yellow arrow: residual bitumen.

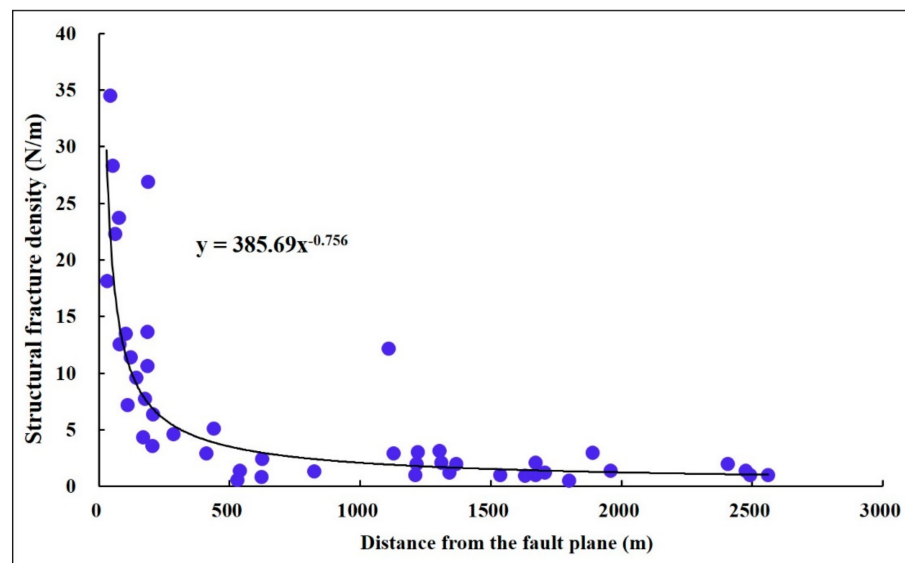


Figure 13. Relationship between fracture density and its distance to fault in the southwest of the Dongying Depression, Bohai Bay Basin. A part of data are taken from [46].

There are differences in the diagenetic process of different formations in a single well. The diagenesis observed in well Bg22 is relatively simple due to the relatively simple lithology of the host rock and the fact that the well did not drill through the Ordovician formation. Controlled by the physical properties of the original lithology, the fracturing widely developed, and the host rock is mostly breccia. Burial dissolution is also well developed in brecciated dolomite formation, which results in higher porosity. Well Bg22 coring is incomplete due to strong fracturing and dissolution. The main cements in well Bg22 are saddle dolomite and anhydrite. A small amount of fine-crystalline dolomite formed in deeper strata. Anhydrite cements formed in the evaporative phase can be observed in the fractures of the dolomite development strata (Figure 14).

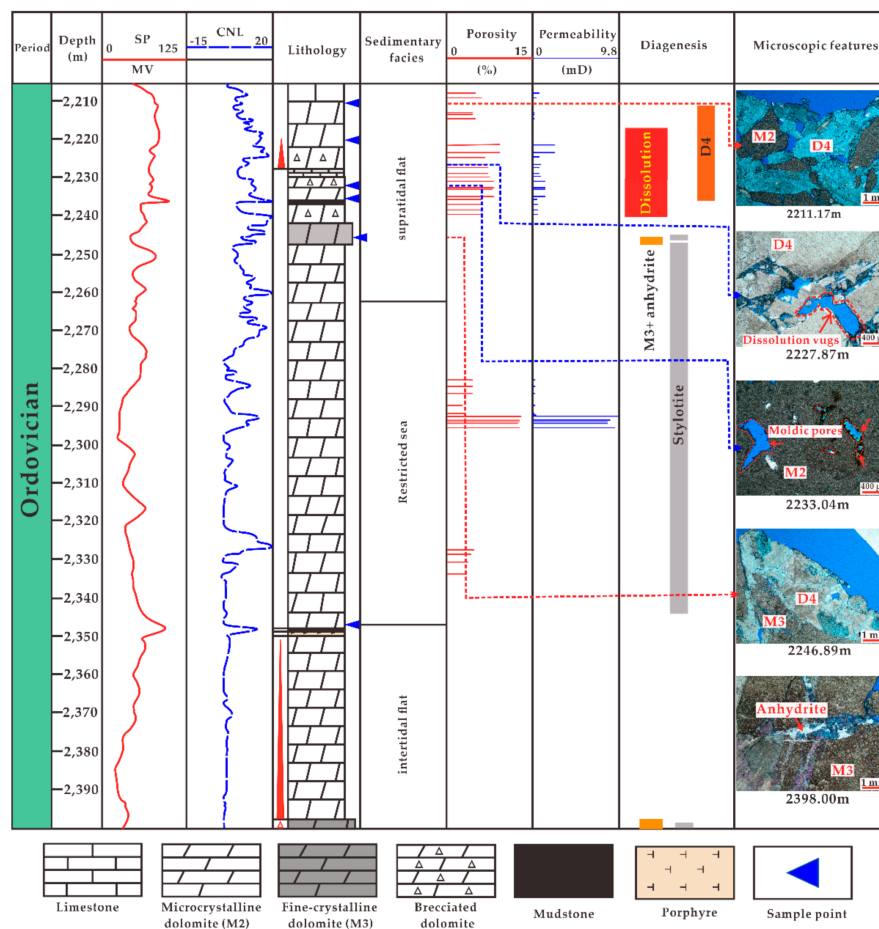


Figure 14. The stratigraphic log of well Bg22 and differences of diagenesis in different strata. M1: argillaceous dolomite; M2: microcrystalline dolomite; M3: fine-crystalline dolomite; D4: saddle dolomite.

In well Bg26, dissolution mainly occurs in the Ordovician strata close to unconformity and faults. In the Cambrian strata, oolitic limestone and bioclastic limestone with better original porosity also have obvious dissolution. Stylolites formed by pressure solution are developed in the Ordovician and Cambrian strata. However, the density of the stylolites in the Ordovician strata are higher than that of the Cambrian strata. Dolomitization is widely developed in well Bg26 and the main products are powder-to-fine dolomite cements (D1). With the increase in the burial depth, the properties of the powder-to-fine-crystalline dolomite cements (D1) change obviously. The crystal size gradually increases. D1 is usually associated with stylolites or formed dolomite patches in the Ordovician strata, while in the Cambrian strata, D1 is mainly filled in oolitic or bioclastics due to changes in the depositional environment. D2 and D3 are products of hydrothermals, so D2 and D3 are

developed in Cambrian strata close to the intrusion, and are widely developed in the Gushan and Zhangxia formation (Figure 15).

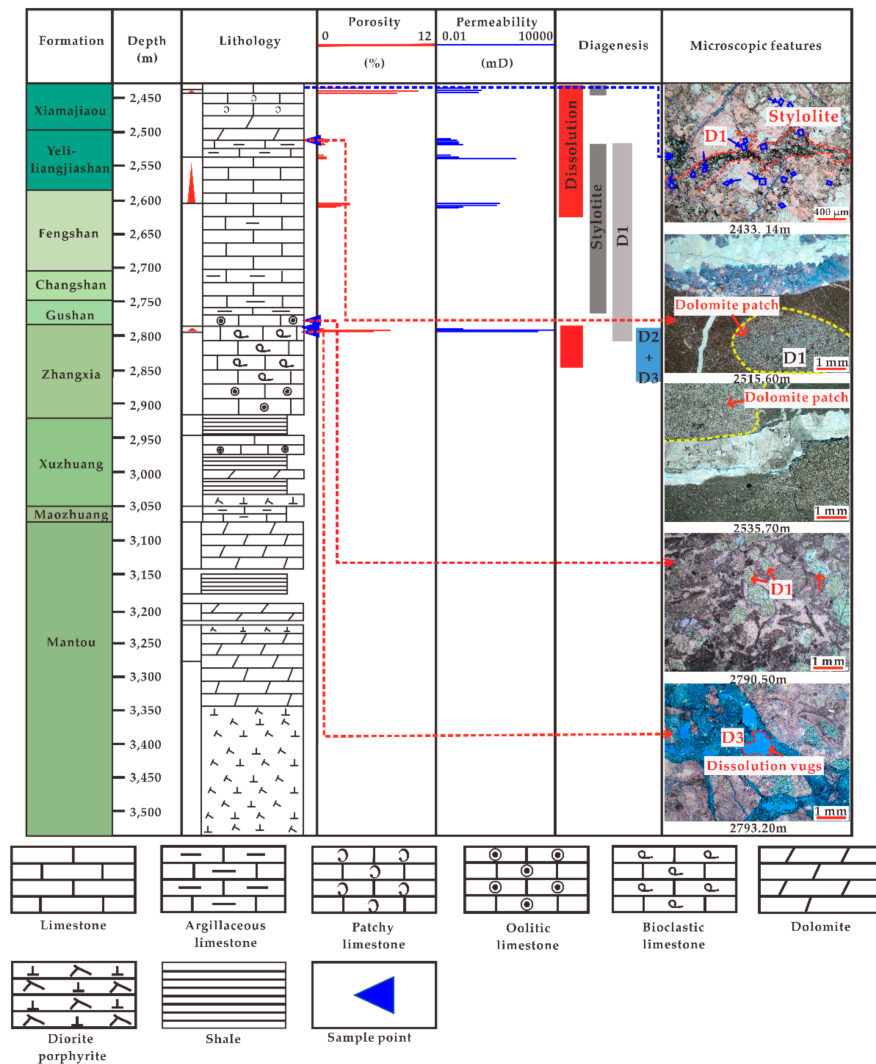


Figure 15. Differences of diagenesis in different strata in well Bg 26. D1: powder-to-fine-crystalline dolomite cements; D2: fine-crystalline ferroan dolomite cements; D3: medium-to-coarse-crystalline dolomite cements.

Four wells (Bg26, Bg22, Bgx15, Bg11) were selected for the study. Bg26 is the closest to the Gaoqing-pingnan fault and oil-generating zone, and suffered the most complicated diagenesis. Dolomitization products are power-to-fine-crystalline dolomite filling inside the oolitic or associated with the stylolites (Figures 15 and 16a). In the Yeli-Liangjiashan formation, dolomitization results in the formation of patchy dolomite in micritic limestone (Figure 16b). Well Bg26 was more easily affected by the hydrothermal fluids and organic acid. The hydrothermal fluid cement associated with dolomite are mainly fine-crystalline dolomite cement (D2) and medium-to-coarse-crystalline dolomite cement (D3) (Figure 16c). Organic acid dissolution is most obvious in well Bg26 due to it is closest to the oil-generating depression (Boxing depression). Well Bg22 did not drill through the Ordovician formation. Bg22 is located in a higher tectonic position than Bg26, and the sedimentary environment is dolomitic flat with strong evaporation for a period of time and forms dolomite with higher original porosity and brittleness. Additionally, the high tectonic position and development of the unconformity plane ensures the host dolomite is easily affected by meteoric water, and it is dissolved by meteoric water to form pores and fractures, which also makes the host dolomite have the geochemical characteristics of meteoric water. Then, hydrothermal fluids

enter the dolomite reservoirs along these pores or fractures. Hydrothermal fluids react with the host dolomite and precipitate saddle dolomite cement (D4) with meteoric water geochemical characteristics in the fractures and pores (Figure 16d). Due to dolomite's high mechanical fracture strength, it is affected by both hydrothermal and tectonic processes. In well Bg22, the fracturing is obvious and the overall coring is incomplete. Well Bgx15 did not drill through the Ordovician formation. Selective dissolution pores are developed in the Ordovician microcrystalline dolomite, forming moldic pores (Figure 16e).

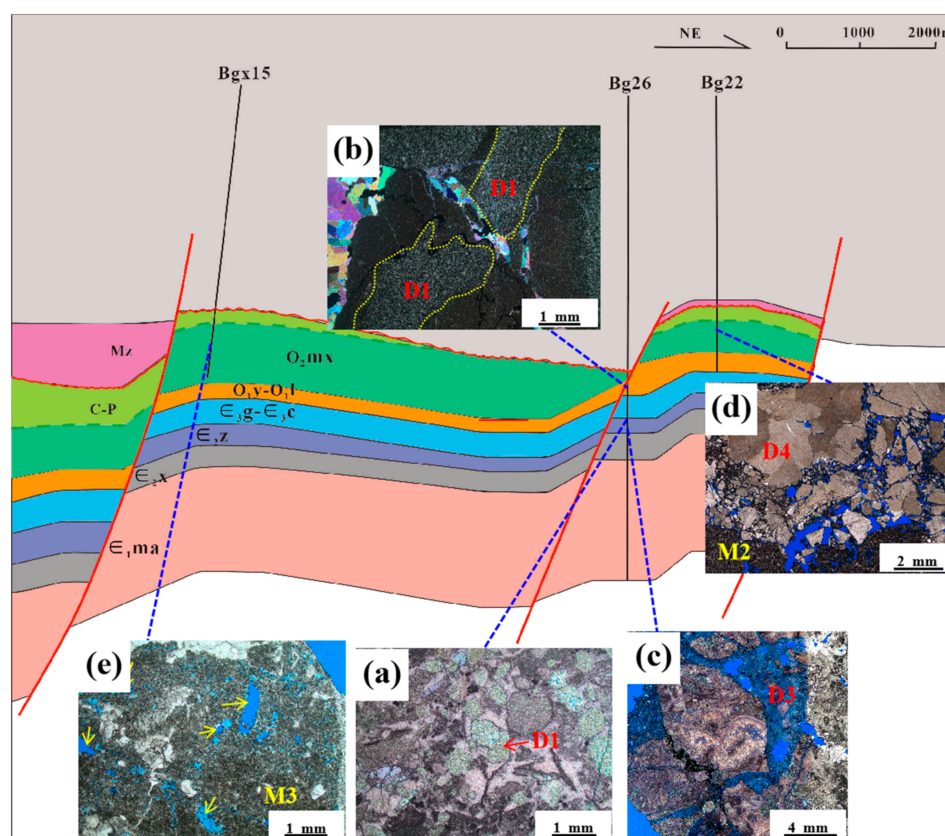


Figure 16. The difference of diagenesis between different wells. (a) Oolitic limestone, Well Bg26 2790.5 m, Zhangxia formation; (b) argillaceous limestone, well Bg26 2540 m, Yeli-Liangjiashan formation; (c) bioclastic limestone, well Bg26 2793.2 m, Zhangxia formation; (d) microcrystalline dolomite, well Bg22 2227.87 m Ordovician formation; (e) microcrystalline dolomite, well Bgx15 2238.9 m, Ordovician formation, moldic pores (yellow arrow); M2: microcrystalline dolomite; M3: fine-crystalline dolomite; D1: powder-to-fine-crystalline dolomite cement; D3: medium-to-coarse-crystalline dolomite cement; D4: saddle dolomite.

6. Conclusions

The following conclusions can be drawn based on petrographic and geochemical investigations of the dolomites at the Lower Paleozoic Formation in the southwest of the Dongying Depression, Bohai Bay Basin:

(1) Dolomites can be divided into the matrix dolomite and dolomite cements. The diagenetic fluid of matrix dolomite is mainly seawater. Dolomite cements can be divided into powder-to-fine-crystalline dolomite cement (D1), fine-crystalline ferroan dolomite cement (D2), medium-to-coarse-crystalline dolomite cement (D3), and saddle dolomite (D4). The powder-to-fine-crystalline dolomite cement (D1) could form by the seepage reflux of sea water or Mg-enriched pore fluids followed by recrystallization during the burial period. The fracture filling dolomite cements, such as D2 and D3 are most likely related to the mixed fluids formed by hydrothermal fluid erosion of the ^{87}Sr -enriched feldspar sandstone in the Maozhuang and Xuzhuang formation. Under the hydrothermal conditions, the host

dolomite formed by the evaporative phase was dissolved by hydrothermal fluids, then Mg-enriched fluid precipitation to form saddle dolomite, resulting in saddle dolomite with the negative $\delta^{18}\text{O}$ value.

(2) The results of the petrology show that there are six types of diagenesis: dolomitization, dissolution, fracturing and cementation, compaction, and pressure solution. Diagenesis in different diagenetic environments has different effects on reservoirs.

(3) Faults and fracture systems are key control factors for dolomite reservoirs and can be used as effective reservoir spaces. The stronger the tectonic activity is, the more faults develop, and the higher the fracture density, the more high-quality reservoirs can be formed. In addition, faults can be used as effective migration channels for fluids that are helpful for later dissolution.

(4) Hydrothermal fluid dissolution and organic acid dissolution result in dolomite reservoirs having better reservoir performance. Due to the late action time of organic acid dissolution, the dissolution vugs can be well preserved. In the study area, organic acid dissolution contributes more than hydrothermal dissolution.

Author Contributions: Conceptualization, X.Z. and Q.L.; methodology, X.Y.; software, L.W.; validation, A.J.; formal analysis, X.Y.; investigation, L.W.; resources, W.T.; data curation, A.J.; writing—original draft preparation, X.Z.; writing—review and editing, Q.L.; visualization, X.Z.; supervision, L.M.; project administration, Q.L.; funding acquisition, L.M. All authors have read and agreed to the published version of the manuscript.

Funding: This research was funded by the National Natural Science Foundation of China (grant number 41602137, 41972107), the National Natural Science Foundation of China (grant number U19B6003), the Strategic Cooperation Technology Projects of CNPC and CUPB (grant number ZLZX2020-02), and the Science Foundation of China University of Petroleum, Beijing (grant number 2462020YXZZ022).

Institutional Review Board Statement: Not applicable.

Informed Consent Statement: Not applicable.

Data Availability Statement: All data used in this research are easily accessible by downloading the various documents appropriately cited in the paper.

Acknowledgments: The authors greatly appreciate the Exploration and Production Research Institute of Shengli Oilfield Company for providing samples and data access and for permission to publish the results.

Conflicts of Interest: The authors declare no conflict of interest.

References

1. Bai, G.P. Distribution patterns of giant carbonate fields in the world. *J. Palaeogeogr. (Chin. Ed.)* **2006**, *8*, 241–250.
2. Halbouty, M.T. Giant Oil and Gas Fields of the Decade 1990–1999. AAPG Memoir. In Proceedings of the 4th AAPG Conference, Denver, CO, USA, 7–10 April 1991.
3. Zhao, W.Z.; Shen, A.J.; Zheng, J.F.; Qiao, Z.F.; Wang, X.F.; Lu, J.M. Discussion on pore genesis of dolomite reservoirs in Tarim, Sichuan and Ordos Basin and its guiding significance to reservoir prediction. *Sci. Sin.* **2014**, *44*, 1925–1939.
4. Zhang, J.T.; Jin, X.H.; Gu, N.; Bian, C.R.; Yang, J.Q.; He, Y.L. Differences and development patterns of karst reservoirs in Majiagou Formation, northern Ordos Basin. *Oil Gas Geol.* **2021**, *42*, 1159–1168.
5. Hao, Y.; Zhou, J.G.; Zhang, J.Y.; Ni, C.; Gu, M.F.; Xin, Y.G. Characteristics and controlling factors of dolomite reservoir of Middle Permian Qixia Formation in northwest Sichuan Basin. *Sediment. Geol. Tethyan Geol.* **2013**, *33*, 68–74.
6. Hu, A.P.; Pan, L.Y.; Hao, Y.; Shen, A.J.; Gu, M.F. Origin, Characteristics and Distribution of Dolostone Reservoir in Qixia Formation and Maokou Formation, Sichuan Basin, China. *Mar. Orig. Pet. Geol.* **2018**, *23*, 39–52.
7. Shu, X.H.; Zhang, J.T.; Li, G.R.; Long, S.X.; Wu, S.X.; Li, H.T. Characteristics and genesis of hydrothermal dolomites of Qixia and Maokou Formations in northern Sichuan Basin. *Oil Gas Geol.* **2012**, *33*, 442–448.
8. Zhu, Y.D.; Jin, Z.Y.; Sun, D.S.; Deng, Y.M.; Zhang, R.Q.; Yuan, Y.R. Hydrothermal dolomitization of Sinian Dengying Formation in south China and its influence on reservoir formation: A case study of Central Guizhou Uplift. *Chin. J. Geol. (Sci. Geol. Sin.)* **2014**, *49*, 161–175.
9. Ma, Y.S.; Guo, T.L.; Zhao, X.F.; Cai, X.Y. Formation mechanism of deep high-quality dolomite reservoir in Puguang Gasfield. *Sci. Sin.* **2007**, *37*, 43–52.

10. Zheng, H.R.; Wu, M.B.; Wu, X.W.; Zhang, T.; Liu, C.Y. Oil-gas exploration prospect of dolomite reservoir in the Lower Paleozoic of Tarim Basin. *Acta Pet. Sin.* **2007**, *28*, 1–8.
11. Sibley, D.F. *Climatic Control of Dolomitization, Seroe Domi Formation (Pliocene), Bonaire, NA*; The Society of Economic Paleontologists and Mineralogists: East Lansing, MI, USA, 1980; pp. 247–258.
12. Shinn, E.A.; Ginsburg, R.N.; Lloyd, R.M. Recent Supratidal Dolomite from Andros Island, Bahamas. In *Dolomitization and Limestone Diagenesis*; Pray, L.C., Murray, R.C., Eds.; SEPM Society for Sedimentary Geology: Tulsa, OK, USA, 1965; pp. 112–113.
13. Vasconcelos, C.; Bernasconi, S.; Grujic, D.; Tien, A.J.; Mckenzie, J.A. Microbial mediation as a possible mechanism for natural dolomite formation at low temperatures. *Nature* **1995**, *377*, 220–222. [[CrossRef](#)]
14. Vasconcelos, C.; Mckenzie, J.A. Microbial mediation of modern dolomite precipitation and diagenesis under anoxic conditions (Lagoa Vermelha, Rio de Janeiro, Brazil). *J. Sediment. Res.* **1997**, *67*, 378–390.
15. Jiang, L.; Pan, W.; Cai, C.; Jia, L.; Pan, L.; Wang, T.; Li, H.; Chen, S.; Chen, Y. Fluid mixing induced by hydrothermal activity in the ordovician carbonates in Tarim Basin, China. *Geofluids* **2015**, *15*, 483–498. [[CrossRef](#)]
16. Smith, L.B. Origin and reservoir characteristics of Upper Ordovician Trenton–Black River hydrothermal dolomite reservoirs in New York. *AAPG Bull.* **2006**, *90*, 1691–1718. [[CrossRef](#)]
17. Davies, G.R.; Smith, L.B. Structurally controlled hydrothermal dolomite reservoir facies: An overview. *AAPG Bull.* **2006**, *90*, 1641–1690. [[CrossRef](#)]
18. Spencer, C.C.; Mullis, J. Chemical study of tectonically controlled hydrothermal dolomitization: An example from the Lessini Mountains, Italy. *Geol. Rundsch.* **1992**, *81*, 347–370. [[CrossRef](#)]
19. White, T.; Al-Aasm, I.S. Hydrothermal dolomitization of the Mississippian Upper Debolt Formation, Sikanni gas field, northeastern British Columbia, Canada. *Bull. Can. Pet. Geol.* **1997**, *45*, 297–316.
20. Ronchi, P.; Masetti, D.; Tassan, S.; Camocino, D. Hydrothermal dolomitization in platform and basin carbonate successions during thrusting: A hydrocarbon reservoir analogue (Mesozoic of Venetian Southern Alps, Italy). *Mar. Pet. Geol.* **2012**, *29*, 68–89. [[CrossRef](#)]
21. Du, Y.L.; Li, S.Y.; Wang, B.; Zhao, D.Q.; Yang, D.D. Diagenesis of the Lower-Middle Permian Carbonate in the Wuwei-Chaohui area, Anhui Province. *Acta Geol. Sin.* **2011**, *85*, 543–556.
22. Giles, M.R.; De Boer, R.B. Origin and significance of redistributional secondary porosity. *Mar. Pet. Geol.* **1990**, *7*, 378–397. [[CrossRef](#)]
23. Ali, M.Y. Carbonate cement stratigraphy and timing of diagenesis in a Miocene mixed carbonate-clastic sequence, offshore Sabah, Malaysia: Constraints from cathodoluminescence, geochemistry, and isotope studies. *Sediment. Geol.* **1995**, *99*, 191–214.
24. Paradis, S.; Lavoie, D. Multiple-stage diagenetic alteration and fluid history of Ordovician carbonate-hosted barite mineralization, Southern Quebec Appalachians. *Sediment. Geol.* **1996**, *107*, 121–139. [[CrossRef](#)]
25. Heydari, E. Porosity loss, fluid flow, and mass transfer in limestone reservoirs: Application to the Upper Jurassic Smackover formation, Mississippi. *AAPG Bull.* **2000**, *84*, 100–118.
26. Esteban, M.; Taberner, C. Secondary porosity development during late burial in carbonate reservoirs as a result of mixing and/or cooling of brines. *J. Geochem. Explor.* **2003**, *78*, 355–359. [[CrossRef](#)]
27. Wang, L.; Shi, J.A.; Wang, Q.; Wang, J.P.; Zhao, X.; Sun, X.J.; Zhao, L.B. Analysis on main controlling factors of Ordovician carbonate reservoir in southwest margin of Ordos Basin. *Pet. Geol. Recovery Effic.* **2005**, *12*, 10–13.
28. Choquette, P.W.; Cox, A.; Meyers, W.J. Characteristics, distribution and origin of porosity in shelf dolostones; Burlington-Keokuk Formation (Mississippian), US Mid-Continent. *J. Sediment. Res.* **1992**, *62*, 167–189.
29. Xie, G.P. Diagenesis and Porosity Evolution of Crystal Garin Dolomite in the Upper Section of the 4th Member of Leikoupo Formation in the Western Sichuan Depression. *J. Yangtze Univ. (Nat. Sci. Ed.)* **2015**, *12*, 24–26.
30. Mo, J.; Wang, X.Z.; Xie, L.; Zhou, Z.; Lin, G.; Xiong, J.W. Diagenesis and Pore Evolution of Carbonate in Sinian Dengying Formation in Central Sichuan Province. *J. Oil Gas Technol.* **2013**, *35*, 32–38.
31. Lavoie, D.; Jackson, S.; Girard, I. Magnesium isotopes in high-temperature saddle dolomite cements in the lower Paleozoic of Canada. *Sediment. Geol.* **2014**, *305*, 58–68. [[CrossRef](#)]
32. Biehl, B.C.; Reuning, L.; Schoenherr, J.; Lüders, V.; Kulka, P.A. Impacts of hydrothermal dolomitization and thermochemical sulfate reduction on secondary porosity creation in deeply buried carbonates: A case study from the Lower Saxony Basin, northwest Germany. *AAPG Bull.* **2016**, *100*, 597–621. [[CrossRef](#)]
33. Ardiansyah, K.; Hilary, C.; Jack, S.; Peter, K.S.; Adrian, B.; Hamish, R.; Fiona, W.; Cathy, H. Evaluating new fault controlled hydrothermal dolomitization models: Insights from the Cambrian Dolomite, Western Canadian Sedimentary Basin. *Sedimentology* **2020**, *67*, 2945–2973.
34. Huang, S.J.; Wang, C.M.; Huang, B.B.; Zou, M.L.; Wang, Q.D.; Gao, X.Y. Scientific research frontiers and considerable questions of carbonate diagenesis. *J. Chengdu Univ. Technol. (Sci. Technol. Ed.)* **2008**, *35*, 1–10.
35. Liu, W.; Xiao, C.T.; Lv, Y.L. Analysis of Burid-hill Reservoir Forming Conditions in the East Section of South Slope of Dongying Depression. *J. Oil Gas Technol.* **2004**, *26*, 6–7.
36. Ge, X. Buried Hill Reservoir Forming Research of Ordovician System in Caoqiao Oilfield. Master’s Thesis, Ocean University of China, Qingdao, China, 2015.
37. Qiu, Z.J. Study on the Geological Characteristics and Control Factors of Caoqiao Buried Hill Reservoir in Dongying Depression, Shandong. Master’s Thesis, Kunming University of Science and Technology, Kunming, China, 2016.

38. Jiang, W. Characteristics of High-Quality Reservoir of the Paleozoic Carbonate Buried Hills in the Dongying Depression. Master's Thesis, China University of Petroleum (East China), Dongying, China, 2017.
39. Wei, X. Evaluation of Karst Reservoir in the Ordovician Badou Formation in the Zhuanghai Area, Jiyang Depression. Master's Thesis, Chengdu University of Technology, Chengdu, China, 2019.
40. Guo, Y.X. A study on constructive diagenesis of the dolomite reservoir within the Yeli-Liangjiashan Formation In the ZHuanghai area of Jiyang Depression. *Acta Mineral. Sin.* **2021**, *41*, 163–170.
41. Li, C.G. Control of fault systems on oil and gas distribution in Dongying Depression. *Oil Gas Geol.* **1994**, *15*, 87–93.
42. Xiong, Z.; Wang, L.S.; Li, C.; Shi, X.B.; Guo, S.P.; Wang, J. Distribution geotemperature in Dongying Depression, Shengli oil and gas field, North China basin. *Geol. J. China Univ.* **1999**, *5*, 312–321.
43. Jiang, Y.L.; Rong, Q.H. Formation pattern of oil-gas pools and distribution of hydrocarbon in Gaoqing area. *Pet. Geol. Exp.* **1998**, *20*, 14–19.
44. Chen, X.; Cao, Y.C.; Yuan, G.H.; Wang, Y.Z.; Zan, N.M. Origin and distribution model of the lower Paleozoic carbonata reservoirs in Pingfangwang-Pingnan buried hills, Dongying Sag. *J. China Univ. Pet. (Ed. Nat. Sci.)* **2020**, *44*, 1–14.
45. Li, G.Y. *Atlas of China's Petroliferous Basins*; Petroleum Industry Press: Beijing, China, 2002; pp. 58–276.
46. Fan, C.T.; Feng, Y.L.; Fu, J.P. Analysis on conditions and rules of reservoir forming of buried hill in Dongying sag. *Pet. Geol. Recovery Effic.* **2002**, *9*, 35–37.
47. Zan, N.M.; Wang, Y.Z.; Cao, Y.C.; Yuan, G.H.; Chen, X.; Jiang, W.; Zhai, G.H.; Song, M.S. Characteristics and development of reservoir space of the Lower Paleozoic buried hills in Dongying Sag, Bohai Bay Basin. *Oil Gas Geol.* **2018**, *39*, 355–365.
48. Lin, S.H.; Wang, H.; Zhang, G.X.; Wu, Y.X.; Chen, H.Y.; Wei, H.B. Pool features of buried hill in west part of Dongying Depression. *Oil Gas Geol.* **2000**, *21*, 360–363.
49. Tian, Y.M. Structural Evolution and Oil-Gas Accumulation Analysis of Buried Hill in the South of Dongying Sag, Bohaiwan Basin. Master's Thesis, Chengdu University of Technology, Chengdu, China, 2005.
50. Machel, H.G. Saddle dolomite as a by-product of chemical compaction and thermochemical sulfate reduction. *Geology* **1987**, *15*, 836–940. [[CrossRef](#)]
51. Dun, T.J. Reservoir research status and development trend. *Northwestern Geol.* **1995**, *16*, 1–15.
52. Xue, H.; Han, C.Y.; Xiao, B.Y.; Han, J.Y. Origin of Reservoirs in the Lower Cambrian Xiaerbulak Formation, Tarim Basin. *Acta Sedimentol. Sin.* **2019**, *43*, 79–88.
53. Jin, C.G.; Liu, J.W. Characteristics of Ordovician Karst reservoir in southern Zhidan, Ordos Basin. *Ground Water* **2016**, *38*, 239–241.
54. Yang, N.; Lü, X.X.; Pan, W.Q. Feature of fracture development in Ordovician carbonate reservoir of Lunnan burial hill. *J. Xi'an Shiyou Univ. (Nat. Sci. Ed.)* **2004**, *19*, 40–42.
55. Zhao, J.L.; Gong, Z.W.; Li, G.; Feng, C.Y.; Bai, X.; Jian, J.; Fu, B.; Hong, Y. A review and perspective of identifying and evaluating the logging technology of fractured carbonate reservoir. *Prog. Geophys.* **2012**, *27*, 537–547.
56. Burke, W.H. Variation of seawater ⁸⁷Sr/⁸⁶Sr throughout Phanerozoic time. *Geology* **1982**, *10*, 516–519. [[CrossRef](#)]
57. McArthur, J.M.; Howarth, R.J.; Bailey, R.T. Strontium Isotope Stratigraphy: LOWESS Version 3: Best Fit to the Marine Sr-Isotope Curve for 0–509 Ma and Accompanying Look-up Table for Deriving Numerical Age. *J. Geol.* **2001**, *109*, 155–170. [[CrossRef](#)]
58. Gregg, J.M.; Shelton, K.L. Dolomitization and dolomite neomorphism in the back reef facies of the Bonnetterre and Davis formations (Cambrian), southeastern Missouri. *J. Sediment. Res.* **1990**, *60*, 549–562.
59. Land, L.S. The application of stable isotopes to studies of the origin of dolomite and to problems of diagenesis of clastic sediments. In *Stable Isotope in Sedimentary Geology (SC10)*; Arthur, M., Anderson, T., Kaplan, I., Veiser, J., Land, L., Eds.; The Society of Economic Paleontologists and Mineralogists (SEPM): Tulsa, Oklahoma, USA, 1983; Chapter 4.
60. Veizer, J.; Bruckschen, P.; Pawellek, F.; Diener, A.; Ala, D. Oxygen isotope evolution of Phanerozoic seawater. *Palaeogeogr. Palaeoclimatol.* **1997**, *132*, 159–172. [[CrossRef](#)]
61. Friedman, I.; O'Neil, J.R. *Compilation of Stable Isotope Fractionation Factors of Geochemical Interest*; United States Government Printing Office: Washington, DC, USA, 1977; Volume 440, Chapter KK.
62. Kinsman, D.J.J. Gypsum and anhydrite of recent age, Trucial Coast, Persian Gulf. *North. Ohio Geol. Soc. Clevel. Ohio* **1966**, *1*, 302–326.
63. Machel, H.G. Concepts and models of dolomitization: A critical reappraisal. *Geol. Soc. Lond. Spec. Publ.* **2004**, *235*, 7–63. [[CrossRef](#)]
64. Adams, J.E.; Rhodes, M.L. Dolomitization by seepage refluxion. *AAPG Bull.* **1960**, *44*, 1912–1920.
65. Wang, S.H.; Song, G.Q.; Xu, C.H.; Chen, L. Early Palaeozoic Sedimentary Facies in the Shengli Oil Province, North China Platform. *Sediment. Facies Palaeogeogr.* **1997**, *17*, 34–40.
66. Sibley, D.F.; Gregg, J.M. Classification of dolomite rock textures. *J. Sediment. Res.* **1987**, *57*, 967–975.
67. Merino, E.; Canals, À. Self-accelerating dolomite-for-calcite replacement: Self-organized dynamics of burial dolomitization and associated mineralization. *Am. J. Sci.* **2011**, *311*, 573–607. [[CrossRef](#)]
68. Dunnington, H.V. Stylolite development post-dates rock induration. *J. Sediment. Res.* **1954**, *24*, 27–49. [[CrossRef](#)]
69. Tang, J.C.; Chen, H.H.; Wang, J.H.; Chen, K.Q.; Qi, K.L. The Diagenesis of the Upper Paleozoic Carbonate Rocks in the Southeast Xiang Depression. *J. Southwest Pet. Univ. (Sci. Technol. Ed.)* **2007**, *29*, 43–46.
70. Beaudoin, N.; Koehn, D.; Lacombe, O.; Lecouty, A.; Billi, A.; Aharonov, E.; Parlangeau, C. Fingerprinting stress: Stylolite and calcite twinning paleopiezometry revealing the complexity of progressive stress patterns during folding—The case of the Monte Nero anticline in the Apennines, Italy. *Tectonics* **2016**, *35*, 1687–1721. [[CrossRef](#)]

71. Veizer, J.; Ala, D.A.K.; Bruckschen, P.; Buhl, D.; Bruhn, F.; Carden, G.A.F.; Diener, A.; Ebner, S.; Godderis, Y. $^{87}\text{Sr}/^{86}\text{Sr}$, $\delta^{13}\text{C}$ and $\delta^{18}\text{O}$ evolution of Phanerozoic seawater. *Chem. Geol.* **1999**, *161*, 59–88. [[CrossRef](#)]
72. Friedman, G.M. Highest Phanerozoic strontium isotopic ratios of pre-rift Late Cambrian passive margin in New York State, USA: Products of continental weathering and orogenesis. *Sediment. Geol.* **2002**, *147*, 143–153. [[CrossRef](#)]
73. Gregg, J.M.; Sibley, D.F. Epigenetic dolomitization and the origin of xenotopic dolomite texture. *J. Sediment. Res.* **1984**, *54*, 908–931.
74. Zhang, J.T.; He, Y.L.; Yue, X.J.; Sun, Y.P.; Jin, X.J. Genesis of iron-rich dolostones in the 5th member of the Majiagou Formation of the Ordovician in Ordos Basin. *Oil Gas Geol.* **2017**, *38*, 776–783.
75. Zheng, C.B.; Zhang, G.S.; Wang, F.Y. Hot Water Karst Characteristics of Ordovician Period in Ordos Basin. *Acta Sedimentol. Sin.* **2001**, *19*, 524–529.
76. He, P.W.; Xu, W.; Zhang, L.J.; Fu, M.Y.; Wu, D.; Deng, H.C.; Xu, H.L.; Sun, Q.M. Characteristics and Genetic Mechanism of Qixia Formation Dolomite in Moxi-Gaoshiti Area, Central Sichuan Basin. *Acta Sedimentol. Sin.* **2021**, *39*, 1532–1545.
77. Li, P.L.; Zhang, S.W.; Wang, Y.S. *Genesis, Accumulation and Exploration of Diversity Buried Hill: A Case Study of Jiyang Depression*; Petroleum Industry Press: Beijing, China, 2003; pp. 30–120.
78. Fisher, R.S.; Land, L.S. Diagenetic history of Eocene Wilcox sandstones, South-Central Texas. *Geochim. Cosmochim. Acta* **1986**, *50*, 551–561. [[CrossRef](#)]
79. Xia, B.; Huang, X.X.; Cai, Z.R.; Jia, H.Y.; Lu, B.F.; Wang, R. Relationship Between Tectonics and Hydrocarbon Reservoirs from Indo-Chinese Epoch to Stage of Yanshan in Jiyang Depression. *Nat. Gas Geosci.* **2007**, *18*, 832–837.
80. Li, D.S. Tectonic pattern of Bohai Bay petroliferous basin. *Pet. Explor. Dev.* **1979**, *2*, 1–10.
81. Kang, Y.; Zou, L.; Liu, Z.Y.; Han, M.; Lu, H.; Yao, S.C. Fault structure and its effect on oil-gas reservoir forming in Qingcheng arch. *Pet. Geol. Recovery Effic.* **2014**, *21*, 45–48.
82. Yang, P.R.; Chen, J.; Cai, J.G.; Yang, H.Y. Structural transitional stages in Jiyang depression and their significance on petroleum geology. *Pet. Geol. Recovery Effic.* **2001**, *8*, 5–7.
83. Qiu, N.S.; Li, S.P.; Zeng, J.H. Thermal History and Tectonic-thermal Evolution of the Jiyang Depression in the Bohai Bay Basin, East China. *Acta Geol. Sin.* **2004**, *78*, 263–269.
84. Faure, G.; Mensing, T.M. *Isotopes: Principles and Applications*, 3rd ed.; Wiley: Columbus, OH, USA, 2004; pp. 363–460.
85. Epstein, S.; Buchsbaum, R.; Lowenstam, H.; Urey, H.C. Revised carbonate-water isotopic temperature scale. *Geol. Soc. Am. Bull.* **1953**, *64*, 1315–1326. [[CrossRef](#)]
86. Grossman, E.L.; Ku, T.L. Oxygen and carbon isotope fractionation in biogenic aragonite: Temperature effects. *Chem. Geol. Isot. Geosci. Sect.* **1986**, *59*, 59–74. [[CrossRef](#)]
87. Smith, L.B.; Davies, G.R. Structurally controlled hydrothermal alteration of carbonate reservoirs: Introduction. *AAPG Bull.* **2006**, *90*, 1635–1640. [[CrossRef](#)]
88. Matthey, D.; Lowry, D.; Macpherson, C. Oxygen isotope composition of mantle peridotite. *Earth Planet. Sci. Lett.* **1994**, *128*, 231–241. [[CrossRef](#)]
89. Wu, Q. Fault System and Tectonic Evolution of Mesozoic-Paleozoic in Gaoqing Area. Master's Thesis, China University of Petroleum (East China), Dongying, China, 2017.
90. Cai, J.X. Characteristics and genesis mechanism of stylolite. *Acta Petrol. Sin.* **1990**, *5*, 51–61.
91. Murray, R.C. Origin of porosity in carbonate rocks. *J. Sediment. Res.* **1960**, *30*, 59–84. [[CrossRef](#)]
92. Waldschmidt, W.A.; Fitzgerald, P.E.; Lunsford, C.L. Classification of Porosity and Fractures in Reservoir Rocks. *AAPG Bull.* **1956**, *40*, 953–974.
93. Qian, Y.X.; He, Y.L.; Chen, Q.L.; Li, H.L.; Lu, Q.H.; Cai, X.R.; You, D.H. Sealing capacity of the Ordovician carbonate rocks in Tazhong area, the Tarim Basin. *Oil Gas Geol.* **2012**, *33*, 1–9.
94. Katz, D.A.; Eberli, G.P.; Swart, P.K.; Smith, L.B. Tectonic-hydrothermal brecciation associated with calcite precipitation and permeability destruction in Mississippian carbonate reservoirs, Montana and Wyoming. *AAPG Bull.* **2006**, *90*, 1803–1841. [[CrossRef](#)]
95. Huang, Q.Y.; Zhang, X.N.; Zhang, S.Y.; Liu, D.; Ye, N. Textural Control on the Development of Dolomite Reservoir: A study from the Cambrian-Ordovician Dolomite, Central Tarim Basin, NW China. *Nat. Gas Geosci.* **2014**, *25*, 341–350.
96. Hou, G.T.; Qian, X.L.; Song, X.M.; Fan, L.X.; Xu, S.G. The Origin of Carbon Dioxide Gas Fields in Jiyang Basin. *Acta Sci. Nat. Univ. Pekin.* **1996**, *32*, 35–41.
97. Zeng, J.H.; Jin, Z.Y.; Zhang, L.P. Mantle-derived fluid activity characteristics and reservoir-forming effect of Gaoqing-Pingnan fault zone in Dongying Depression. *Geol. Rev.* **2004**, *50*, 501–506.
98. Li, Y.; Yan, Y.S.; Song, Z.J.; Tang, Z.Q. Study on Fracture Movement and Petroleum Pool-matured Phases of Pingnan Oilfield—Based on the Evidence of Liquid Inclusions. *J. Shandong Univ. Sci. Technol. (Nat. Sci.)* **2010**, *29*, 14–19.
99. Shang, X.F.; Sun, X.J. The influences of Organic Liquid's on Reservoir Diagenesis-Taking Dongying Sag as an Example. *J. Libr. Inf. Sci.* **2011**, *21*, 184–188.
100. Sun, S.Q. Dolomite Reservoirs: Porosity Evolution and Reservoir Characteristics. *AAPG Bull.* **1995**, *79*, 186–204.
101. Hugman, R.H.H.; Friedman, M. Effects of texture and composition on mechanical behavior of experimentally deformed carbonate rocks. *AAPG Bull.* **1978**, *63*, 1478–1489.